UNIVERSITY OF PADOVA

DEPARTMENT OF MANAGEMENT AND ENGINEERING

MASTER'S DEGREE IN PRODUCT INNOVATION ENGINEERING

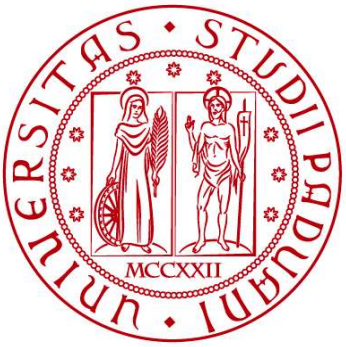

Master's Thesis in Product Innovation Engineering

(Master's degree LM 33 – Mechanical Engineering)

FINITE ELEMENT STRESS ANALYSIS ON NON-FLAT ADHESIVELY BONDED SINGLE LAP JOINTS WITH SINUSOID INTERFACES

Supervisor: Prof. Paolo Ferro

Co-Supervisor: Prof. Filippo Berto

Candidate: MICHELE ZECCHINI

ACADEMIC YEAR 2016 – 2017

Acknowledgments

I would like to express the deepest appreciation to my supervisor and co-supervisor, Professor Paolo Ferro and Professor Filippo Berto, who guided me in drafting this thesis as well as in my Erasmus experience: the climate almost familiar and definitely stimulating that I found in Norway is largely due to their efforts and to their great attitude.

I would like to thank the PhD student that more than any other accompanied me during the analyses, Seyed Mohammed Javad Razavi: more than a collaborator I found in him a supporter and a friend.

I must also mention the NTNU and all the people that contributed in making my stay in Trondheim one of the best experiences of my life: Alessandro, Angelo, Daniele, Davide B., Davide P., Filippo, Giacomo, Luca, Luigi, Mirco, Thomas.

I would like to thank all my family, especially my grandmother and my parents; without their love and patience I would never be able to finish my studies.

Finally, I extend my greatest appreciation to all the friends that played a fundamental role in the journey that led me to this thesis: Cecilia, Daniele e Marta, Francesco e Giorgia, Giada e Silvia, Gianmarco, Giorgia S., Igor, Marco P., Marco Q., Melania, Michael.

Summary

This study explores and describes factors involved in the analysis of an adhesively bonded single lap joint with non-flat sinusoid interfaces, investigating the stresses distributions and the apparent generalized notch stress intensify factors. With the help of a powerful engineering tool like Ansys, different geometries are implemented using four parameters to study the response in terms of ANSIF and to obtain a pattern; these parameters are the length of each wave, the height of the sinusoid, the layer thickness and the elastic modulus of the adherend.

In the end, some interesting conclusion which can be useful for both research and industry are presented and explained, opening to new examinations.

Index

Introduction

The importance of adhesive bonding, the material joining process that uses the solidification of an adhesive placed between the adherend surfaces to produce an adhesive bond, is growing up and its applications are constantly increasing in various fields such as aeronautics, aerospace, electronics, automotive, construction, sports and packaging. This kind of joint is a great alternative to the conventional mechanical fasteners and provides many advantages like a lower structural weight, a lower fabrication cost and an improved damage tolerance.

In the past years, the adhesive joints have been studied by many people with the aid of closed form algebraic techniques of different complexities and considering some of the main factors that affect every kind of adhesive bonded joints: adhesive thickness, material properties of adherends and adhesives, temperature, geometry of the layer and so on.

Fig. 0.1 shows as this technique is widely used in one of the important fields above mentioned, the aeronautic one, illustrating an airplane material composition mainly composed of composite materials and adhesive bonded skins and doublers.

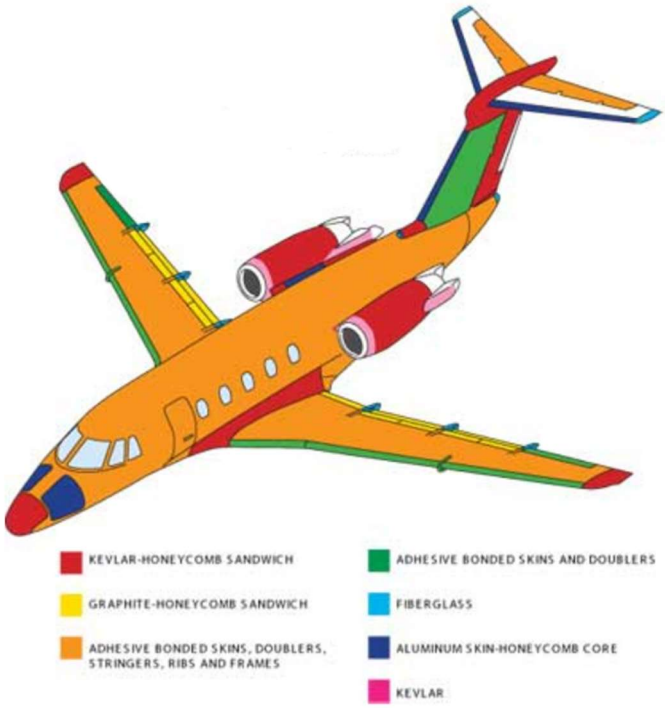

Fig. 0.1. *Airplane composition*

Animal glues and other natural products has been the only known adhesives for many years, though since the end of 19th century some vegetable glues have found their application in bonding porous materials; during World War I casein adhesives were used in wooden construction but they proved to have limited resistance to mould growth and moisture. A solution to this issue has been found in synthetic resins, which do not have the same restrictions of the natural products and which can bond also metals and non-porous materials, main reason for the great increase in the use of adhesives in industry. The first synthetic resin of major importance has been the phenol formaldehyde, largely used in timber bolding, and even today it has a huge field of application, from the manufacturing electrical components like punch-through boards, to the paper composite panels, through the making of countertops. Epoxy resins and new types of phenolic have been developed during World War II for being used in structural metal bonding in aircraft and this marked the start of numerous researches on synthetic resins and rubber. Today adhesive bonding is of great importance for joining metals as well as other materials for many different purposes; the intermediate layer can be applied using spin-ok, spray-on, screen printing, embossing, dispensing or block printing on one or more substrate surfaces. Its thickness can easily change varying the viscosity of the adhesive, the rotational speed or the pressure applied by the tool. Most of the adhesives used in these type of joints are polymers that allow connections between adherends at such low temperatures, ≤ 200 °C, that enable the integration of micro-structures, electronics and metal electrodes on the wafer.

Depending on several factors like the adhesive used, the methods of application, the joint design and the function of the ultimate assembly, adhesive bonding can bring one or more of the listed advantages:

- The opportunity to bond together a large variety of materials, which can differ in compositions, Young's modulus, Poisson's coefficient and thickness (too thin objects would be distorted or destroyed by other methods).
- The ability to avoid irregular surface boundaries produced by processing tools such as screws and rivets, which means a better esthetic of the final assembled.
- The improvement of the stress distributions over the whole bonded area, making them more uniform and minimizing the stress concentrations, like the ones that come from reduced

contact surfaces made by bolts, rivets or spot welds. The chance to use thinner materials without losing strength leads also to cost and weight saving.

- Fine insulation and sealing properties as adhesively bonded joints are insulated through the adhesive layer against heat, sound or electricity, while they are sealed to prevent the damages created by moistures and chemicals; the adhesive layer can also avoid galvanic corrosion between different metals.
- The opportunity to bond together heat-sensitive subjects which would be seriously damaged by brazing or welding.
- The minimization of the weight as well as a better integrity of the structural elements since the presence of holes is not necessary.
- The creation of complex shapes, impracticable with other fastening methods.
- The elastic properties possessed by most of the adhesives and the great damping capacity of adhesives bonds that enable the absorption, distribution and transfer of stresses; this leads to an improvement of the fatigue resistance and gives an excellent vibration damping together with other flexibility properties.
- The achievement of considerable cost savings for both process and final assembly, thanks to the reduction of material requirements, weight and operations like drilling, screw or nut driving and finishing; there are also some simplifications in the assembly procedures as well as other advantages like the substitution of many mechanical fasteners with a single bond and the possibility to join more than one component at the same time.

Bonded joints are usually expected to stay under static or cyclic stresses for long periods of time without losing any property concerning the load-bearing capacity of the structure; the lack of models and failure criteria led to the ‘overdesign’ of composite structures, including mechanical fasteners as safety precaution and resulting in heavier and more costly components. For these reasons the research is constantly trying to improve the knowledge in such an important field, connected to many different applications.

In the same way, the absence of a proper three-dimensional analysis in the field of bonded joints led to the development of many experiments and papers on this particular topic, showing that

it is possible to find out the value of out-of-plane stresses instead of overlook them or estimate them.

These stresses have always been considered of minor importance not only for their size, smaller than the in-plane ones, but also for the difficulty of calculating them using a three-dimensional model in programs like ANSYS® or ABAQUS®. They have hardly ever been calculated accurately but, when considered, they have always been estimated from other parameters such as the distribution of stresses along the other two remaining directions, the orthogonal one and the tangential in-plane one. Most of the three-dimensional analyses require a huge amount of RAM and time from the analyzer if compared to the classic two-dimensional models, but that is no more a problem thanks to the progresses made in this field that provide always better computers. Furthermore, the review of the strain energy density approach applied to V-notches and wielded structures made by professors Lazzarin and Berto [1] has become a powerful and useful tool in this situation, making it possible to fully reproduce the complexity of a real specimen in a virtual machine.

The work done to date with the aim of optimizing the bonded joints could be divided into two different macro-groups: the researches made on the nature of the joining materials and the ones made on the geometry; both of them have been studied, most of the times using two-dimensional models. The second group has given rise to many variants of the adhesively bonded flat joint, like the ones with wave or zigzag interface, characterized by many parameters that can be studied and used to obtain a stronger joint.

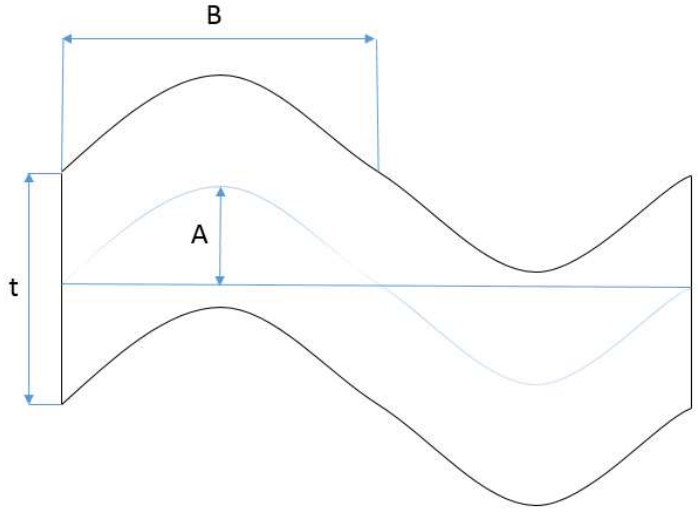

Fig. 0.2. *Parameters of a non-flat sinusoid adhesive layer*

This is the contest where the present thesis takes place, inspired by the previous works on two- and three-dimensional analyses of bonded joints, especially the adhesively bonded single lap joints, and by the theoretical studies on fracture mechanics and on innovative materials. The main objective is to deeply analyze the influence of different surface geometries on the in-plane and out-of-plane stress distributions in adhesively bonded single lap joints. The more efficient wavy joint will be analyzed, as well as different wavy geometries will be compared with each other to find out the best parameters in terms of number and height of the waves (Fig. 0.2). In the first round of simulations the same amount of pressure will be applied to the same joint changing the number of waves from two to six and choosing between five different paths along the width will be analyzed, from the surface of the specimen to its center; for every path the stress intensity factor will be calculated considering only the results which are meaningful and comparable with each other. In the end, every apparent generalized notch stress intensity factor (K_1^{app}, K_2^{app} and K_3^{app}) of the same geometry will be used to find out a valid pattern that can be compared with the ones of different wave lengths. A similar analysis will be repeated using A, the height of the waves, as a parameter instead of B, the length of each wave: only the geometries with a negative slope will be considered, in fact these are the more efficient ones according to the literature, and the height of each wave will change from -0.5 mm to -3.0 mm; this second part of the work will lead to more complex and complete considerations. In the end a third analysis will be led on the same geometry studying the differences that arise when the thickness of the adhesive layer changes from 0.2 mm up to 0.6 mm. The last parameter used will be the Young's modulus of the joint, which will assume values between 40 GPa and 200 GPa.

There are some other important factors that could be considerate with these three, such as new materials for adhesive and adherends, but some of them have already been considerate in previous works while others can be analyzed in an eventual extension of the present research. It would also be interesting to have a physical match to compare to the computer simulation made.

This thesis has been divided into four chapters, not counting the other paragraphs and appendices as this introduction or the references.

The first chapter starts as a short review of the main works concerning the topics of general bonded joints, single-lap and multi-lap joints, the hypothetical improvements that can be achieved

operating on materials or geometry and the differences between flat and non-flat joints; instead, the second part of this section is a focus on the differences between two-dimensional and three-dimensional studies and on the reasons why the last ones have been studied just in the last years. The review will consider the papers made on the effects of an in-plane stress applied to a three-dimensional joint, analyzing all the out-of-plane effects that are generated in the volume and that are usually underestimate.

The second chapter illustrates the finite element method used to simulate the application of stresses to different geometries of joints: every choice made during the pre-analysis phase will be reported and explained, like the ones correlated to the size and to the shape of the elements or like the boundary conditions. This section reports also formulas and graphics necessary to obtain the K_i values that will be used in the next part of the thesis, that are the factors symbolizing the intensification of the stresses in a particular direction.

The third chapter concerns about the elaboration and the discussion of the results obtained from the previous analyses, comparing the cases of different geometries and trying to deduce a scheme from them, with the help of literature and of other works made on the same topic. In a first moment, only the number of waves is used as a parameter for the analyses, while in the second part of this chapter the height of the sinusoidal waves will change too, even though it will always be maintained negative to achieve greater benefits in terms of stress distribution. During the third section the thickness of the layer will be increased up to three times the initial one while analyzing the variations produced on the stress distribution. Lastly, the fourth part of this chapter analyzes the effects of a parametric study on the adherend's elastic modulus.

The fourth and last chapter is the one that reports all the conclusions and the deductions made from the elaboration of the data and tries to place these results in the context of current scientific research. Some important relations are explained and justified thanks to the graphics and the distributions of values from the previous chapters.

Chapter 1

State-of-the-art

This chapter is a summary drawn from the current state of the literature on joints, especially the adhesively bonded ones. It will be briefly treated the major works carried out to date, from those related to the material analysis up to those which studied the design to optimize the joint strength. The last ones will be discussed in a more accurately way as they are closely linked to the subject of this thesis.

1.1 Previous analyses of single lap joints

Joining two structural materials, the geometric or elastic discrepancies generate a complex state of deformation and concentrated stresses along the boundary. These discontinuities may facilitate the initiation and propagation of defects and cracks, compromising the effectiveness of the joint.

The limiting factor in many bonded systems is the adhesive layer, because its properties are weaker than the ones of the adherent; Davis and Bond studied this issue in the aeronautic field, where the variability of adhesively bonded joints was nearly unpredictable. These problems were usually related to the lack of understanding of the adhesive bonding processes: in [2] some basic principles have been detailed to obtain strong, durable and more predictable adhesive bonds. Sheppard et al. [3] instead studied the singularities at the ends of the joint when there was still no suitable failure criteria. They proposed a damage zone model which achieved a good correlation with the experimental results, as well as another modified version of this damage zone that allows the implementation of the model in engineering analysis.

Some suggestions to solve these problems can be found in nature like in the example of the nacre or mother-of-pearl, which is a nano-composite of ceramic and biopolymer with extraordinary mechanical properties [4, 5, 6]. Its strength is mostly related to interlocking ‘wave

shape' polygon tablets that slow the propagation of cracks distributing them along the whole structure. This solution underline the great importance of boundary's geometry in every kind of joint.

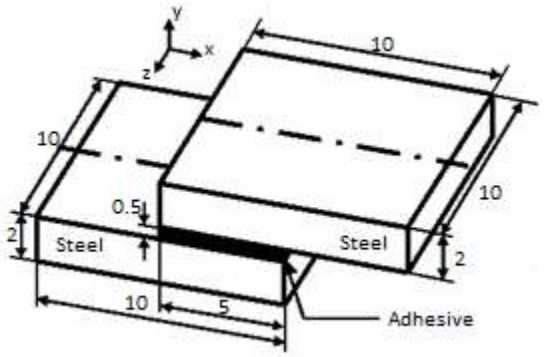

Fig. 1.1. *Example of single lap joint*

In the last years, the adhesively bonded joints replaced other methods of joining like welding, bolting and riveting in many different industries. The most common methods of bonding using an adhesive material are the single lap adhesively bonded joints, or SLJ, especially useful because of its ease of application and its low price, and the double lap joint, with two bondlines. The double lap joint is the simpler type to analyze because there is no bending during deformation, but the single lap joint is the one of more practical importance Its characteristics make it attractive in fields such as aeronautics, automotive and civil engineering: when compared to mechanically fastened joints, the adhesive ones have many advantages also related to less sources of stress concentrations, more uniform distribution of load and better fatigue properties. The single lap adhesively bonded joints is characterized by two main problems: the geometry of the joint gives rise to a bending moment which weights the local stresses at each end of the bonded region and transfers in an ineffective way the load; in addition the stress distribution varies along the region of the adhesive, with peak values on its ends. Adhesive properties proved to be the limiting factor in most cases, stimulating the development of better adhesives and surface treatments to change the structure of the adherent surface, as well as geometric modifications.

In [7] Xiaocong made a good review of finite element analysis of adhesively bonded joints with different designs (Fig. 1.2) in terms of static loading analysis, environmental behaviors, fatigue loading analysis and dynamic characteristics. The author underlines the vital importance of

finite element analysis in this fields, explaining that it will help future applications of adhesive bonding by allowing system parameters to be selected in order to give a larger process window for successful joint manufacture. Furthermore the computer analysis allow many different designs to be simulated before testing them in the laboratories, saving a huge amount of time.

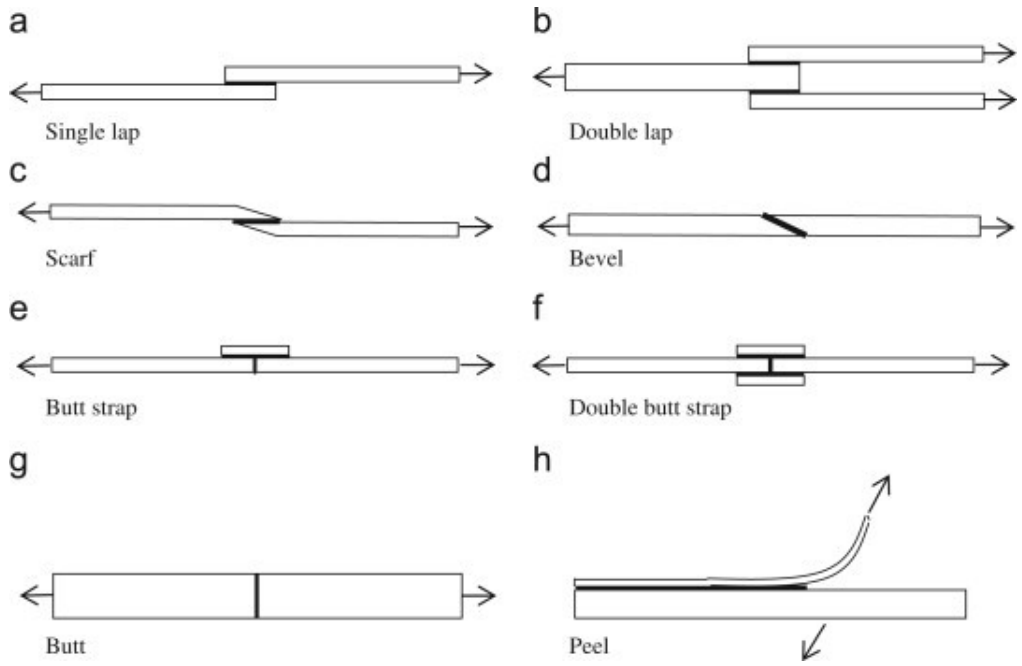

Fig. 1.2. *Some common engineering adhesive joints [7]*

The paper of Belingardi et al. [8] covers the topic of geometric modifications and explains how the geometry of the layer is an important factor for these peak values: it has been demonstrated that the use of spews and chamfers with an angle of about 45° leads to a considerable reduction of the stress peaks. A large number of works have been carried out since the second half of the twentieth century to find out different solutions to optimize the joint strength of single lap joints, Cooper et al. [9] for example used finite-element, Goland-Reissner and photoelastic analyses that show how for a single lap joint the geometric nonlinear behavior has a sizable effect on the stresses in the adhesive; the Goland-Reissner analysis was a good method to predict the stresses along the midsurface of the adhesive bond to study the influence of geometric and material parametric

variations. The same paper also provided a basis of stress distributions in both the adherents and adhesive for comparison with other solution techniques.

The strength of and adhesive joint can be improved by two different methods, ***changing adhesive materials*** (using fibers or other particles into the adhesive or applying a bi-adhesive in the joint) or ***changing the geometry***, which is the topic that this thesis is going to investigate.

1.1.1 Improvement by optimizing the materials

In literature there are many writings about this topic, starting from the works of Erdogan et al. [10] and of Renton et al. [11]: the first one analyzes the stress distribution in plates bonded through stepped joints under the assumption of generalized plane stress for specific plate geometries and material combinations, contemplating also the case of a smoothly tapered joint and comparing it with a stepped joint; the second one focuses on the Young's modulus of the adherend, on the overlap length and on the adhesive's material properties to find out the most influential parameters in optimizing the design of a single lap joint. In the last years, these topics have been deeply studied, Akpinar et al. [12] studied the normal and shear stress distributions occurring in a bi-adhesively bonded T-joint using a non-linear three dimensional finite element analysis and found out that, for a given adherend, lowering the stiffness of the adhesive leads to a lower stress concentration and then to a higher joint strength. In addition, using lower stiffness adhesives at the ends of the bi-adhesive layer can further decrease the stress concentration and increase the joint strength. The reinforcement of the adhesive layer was another topic of great interest; in [13, 14, 15] many types of particles and fibers were added to the joint in order to verify their effects. The analysis of metallic fiber-reinforced adhesively bonded joints underlined the influence of reducing the distance between the fibers, of increasing the fiber diameter and of choosing a stiffer material for fibers: all three contribute in improving the stress distribution and in reducing the maximum and average stress values typical of the adhesive layer.

The effect of graphene nanostructure reinforcement studied by Gultekin et al. [14] is in line with the results of the reinforced methods indicated in literature, a great effect on the failure load of the joint. A new method was also developed, showing a greater failure load of the joint and a major minimization of the standard deviation: these kind of improvements help to improve the

reliability and reproducibility of the joint. The paper in [15] is one of the latest investigation and considers the effect of nanoparticles in the adhesive layer on elongation at failure and on the shear strength: the results indicates an improvement of the adhesion in the joint and different damage mechanisms were observed for different toughening particles. In this case the particle debonding, the shear yielding and subsequent void growth were found as effective mechanisms of energy absorption. Another recent work is the one of Esmaeili et al. [16]: they studied the flexural behavior of metallic fiber-reinforced adhesively bonded single lap joints focusing on some important parameters such as volume fraction, fiber diameter, distance between the fibers, mechanical properties of the fibers and their orientation. They found out that it was possible to reduce the peak normal stresses in the adhesive layer, making the stress distribution more uniform and improving the load bearing of the joint, by increasing the fiber diameter, reducing the distance between the fibers and choosing a stiffer material for the fibers in the longitudinal direction. These are just some of the ways to improve the stress distribution in the adhesive layer as well as increasing adhesive toughness exploiting the material innovations.

1.1.2 Improvement by optimizing the geometry

Different methods have been checked to modify the adhesive joint's geometry by use of chamfering, tapering and rounding the substrates to obtain a reduction of the peak values of normal and shear stresses at the ends of the layer. In [17] a focus on T-joint configurations with embedded or non-embedded supports explains how the variation of the geometry of the bonding zone in the embedded joints changes the stress distribution. This has a strong influence on stress concentrations, prolonged performance and load bearing capacity of these joints: it was founded that, for a given adherent, the lower the stiffness of the adhesive, the lower the stress concentration, obtaining great advantages in terms of joint strength. The paper in [18] analyses the effect of the spew fillet instead (Fig. 1.3), thanks to experimental and 3-D non-linear stress analysis: it shows how the spew fillet in the single lap joint's geometry with different widths helps in decreasing the stress concentrations and in increasing the strength of the joint as well as its load carrying capacity. Another noteworthy work is the one of Akpinar [19] where single lap joints, one step lap joints and

three step lap joints were studied in order to find a way to reduce the stress values at the edges of the overlap area. The one-step lap geometry seemed to reduce the stress concentration but the highest decrease was obtained with the three-step lap geometry. Furthermore, the reduction of the stress values at the edges of the overlap area confirmed the increase of the experimentally obtained load carrying capacity of the joint.

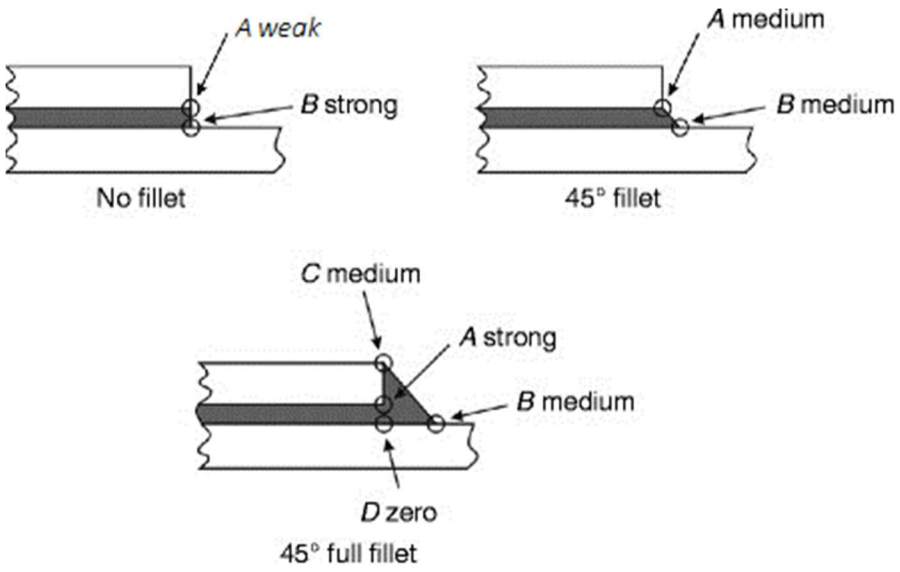

Fig. 1.3. *Different types of fillet [20]*

Tapering the adherends has the same effect, reducing the peel stresses in the layer, increasing the strength of the joint and altering the failure mode, from peel to shear. The documents [21] and [22] study this particular subject in detail and they suggest using external tapers with 30° fillets to reduce significantly the peak values of peel stresses at the ends of the bond line. On the other side, Hildebrand [23] analyzed different geometries of the edges applying the non-linear finite element methods during the analysis of single lap joints of metal with fibre-reinforced plastics (FRP). The modification of the joint ends by tapering, rounding or denting for different combinations of metal adherend/FRP and adherend/adhesive shows that the strength of the joints can be increased by 90-150%, if the design is carefully projected.

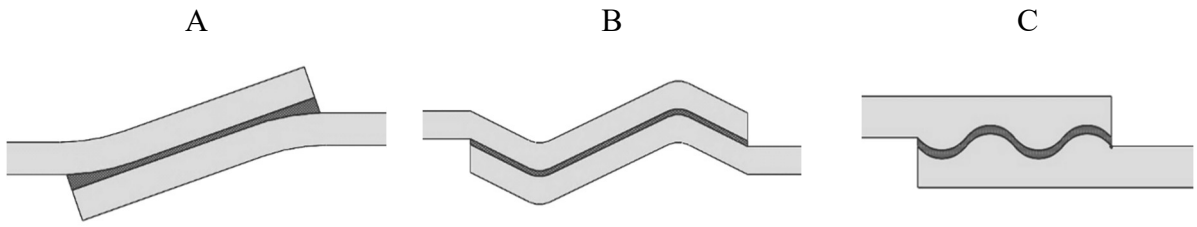

Figure 1.4. *Schematic view of modified single lap joints [24]*
(a) Reverse-bent SLJ, (b) wavy SLJ, (c) SLJ with sinusoid interface

Many researchers tried to introduce local compressive stresses at both ends of adhesive layer and this aim led to the non-flat adhesive joints. Different designs of non-flat adhesive joints are illustrated in Fig. 1.4, among which can be found the reverse-bent single lap joints, the wavy single lap joints and the single lap joints with sinusoid interface. Boss et al. [25] examined the behavior of single-lap adhesive bonded joints with modulus and geometrically adherents: in certain cases, modulus grading reduces the stress level compared to geometrical grading; in other cases they brought benefits similar to geometrically graded adherents. The modulus grading provided better performance in order to reduce the shear stress but a combination of modulus and geometrical grading can lead to even better performing single-lap bonded joints. McLaren et al. [26] proposed to deform the substrate at the border of the overlap length to optimize the stress distribution in the critical area of the joint (Fig. 1.4a) and analyzed it photoelastically. The modified design is called reverse-bend single lap joint and it introduces a bending moment in the substrates opposite to the one produced by the classic single lap joint. The new bending moment helps in diminishing the maximum peel stress and brings to a more uniform shear stress in the adhesive. In [27] the mechanical behavior of composite adherents applied in reverse-bent SLJ was studied through numerical and experimental investigations, comparing them with the traditional single lap joint. The results showed how the strength of the joint depends on the material combinations that are chosen. Furthermore, they studied the fatigue behavior of the new geometry with many yield and plastic deformation characteristics, revealing that the reverse-bent single lap joint has higher efficiency under fatigue loading if compared to the classic single lap joint. The improvements obtained under static tests conditions become significantly higher benefits in fatigue [28]; the same paper also illustrates the failure mechanism of the single lap joints under fatigue loading.

Another work by Campilho et al. [29] considered some reverse-bent aluminum joints made of brittle and ductile adhesive and studied them with both experimental and analytical points of view. The aim once again was to reduce the peel and shear stress concentrations at the overlap edges, which are particularly dangerous when using brittle adhesives because they do not allow plasticization in those regions. They tested different combinations of joint eccentricity trying to optimize the joint with the support of ABAQUS®; the results showed an advantage of using the proposed modification with the brittle adhesive but at the same time the ductile adhesive did not show to be affected by the bending technique. You et al. [30] tested different preformed angles in the lap zone of steel adherends using an elasto-plastic finite element analysis and a scanning electron microscopy. The numerical simulation showed that the peak stresses of the mid-bondline in the adhesive bonded single lap joint were significantly reduced as the preformed deflection angle was increased from 0 degrees to 15 degrees. The highest value of the average ultimate load of the experimental joints occurred with an angle equal to 7 degrees, showing a failure load enhancement about 64% higher than the standard single lap joint. The SEM images also indicated that, in the overlap zone of the joint, the failure mode changed from that of a mainly adhesion one to a mixed one increasing the preformed angle.

In [31] and [32] Zeng and Sun proposed a new model of SLJ called wavy lap joint (Fig. 1.4b) which leads to lower peak stresses at the end of the bon lines compared to the classic single lap joint; this characteristic significantly improve the strength of the joint and its load bearing. In the new design the load eccentricity as well as singular peel stresses in the joint interface were avoided, the peel stress becomes compressive in the joint end region and the shear load is more evenly transferred through the length of the joint. They also performed some comparative fatigue tests [33, 34] on the new geometry to verify the effects of substrate non-flatness and in order to fully demonstrate advantage of the new wavy lap joint. These tests were conducted at different load levels and load frequencies, showing that the wavy lap joint had a longer fatigue life compared to the conventional single lap joint. A similar geometry (Fig. 1.5) has been studied by Avila and Bueno [35] with both numerical and experimental studies using composite substrates, observing not only the sample size population but also the statistical differences with the single lap joints. The results show an increase of nearly 41% on loading that could be due to the compressive stress field created in the joint. In addition, the stress field distribution can be the reason for the delamination of the adherent that occurred in the wavy-lap joints.

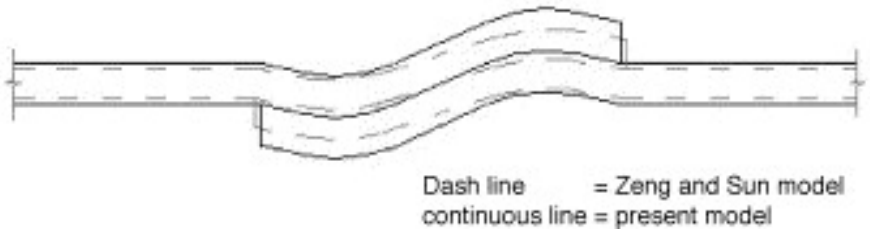

Figure 1.5. *Distinctions between Zeng and Sun's model and Avila and Bueno's model [34]*

Shiva Shankar et al. [36] also proved an improvement of the joint's strength in the wavy geometry. Fessel et al. [37] conducted a comparative analysis of the stresses of the conventional joints, the reverse-bent and the wavy joints using finite element analysis. They carried out a parametric study showing trends influencing stresses in the adhesive layer using different substrate materials, adhesive and overlap lengths. They found that the joint strength of "reverse-bent" joints was up to 40% higher than the flat joints. Moreover, the failure of single lap joints appeared to be due to the peel stress and yielding of the adherends, whereas the wavy and reverse-bent joints mostly failed due to shear stress or to lateral straining of the adherends away from the overlap.

In 2008 De Moura et al. [38] discussed the adequacy of cohesive and continuum mixed-mode damage models applied to the simulation of the mechanical behavior of bonded joints. They presented a cohesive mixed-mode damage model which was appropriate for ductile adhesives and they proposed the end-notched flexure tests and the double cantilever beam to find the cohesive properties of a thin adhesive layer under mode II and mode I, respectively. It was also proposed a new data reduction scheme which was based on the crack equivalent concept in order to overcome crack-monitoring problems during the propagation in these fracture tests. Furthermore they elaborated a continuum mixed-mode damage model to simulate the cases where the thickness of adhesives plays an important role, model that can be used to simulate different shapes of the fracture process zone (FPZ) as a function of adhesive thickness.

Temiz et al. [39] observed the effect of residual stresses induced in the overlap area with certain curvatures. They cured placed the samples with curved overlap area under pressure to flatten the curvature and they cured the adhesive to obtain an adhesive layer with compressive stresses that decrease the effect of peel stress and increases the loading capacity. The results reported a load

bearing capacity about 46% higher than the flat single lap joints; furthermore, the experimental study showed that the overlap length, patch thickness and patch materials have notable influence on the failure strength and displacement capacity of the joints. Akpinar et al. [40] used the same method provided by Temiz and al. on the adhesively bounded double strap joints: since the elastic adherend overlap ends tend to revert to the initial curved form, they create a compressive residual stress distribution on the adhesive layer. These induced residual stresses increased the strength of single lap joints subjected to tension; they obtained an enhancement of the failure load capacity up to 38%. The effects of overlap length, patch thickness and patch materials on the bond strength have been deeply studied by Akpinar founding a considerable influence on both displacement capacity and failure strength of the joint.

These non-flat single lap joints have a big limitation related to their field of application: they cannot be used in thick adherends but only in the thin ones. A common way to improve the locking and adhesion between the adhesive and the adherends is by roughening of the adherend surface before bonding the materials, as it is explained in [41]. An abrasion treatment significantly increases the joint strength unlike changing the linear directions of this abrasion. However, roughening the surface does not have a great effect on the load transfer due to the small dimensions of the surface roughness. This led to a different method to improve the load bearing of adhesive joints with both thin and thick adherends, varying only the interface shape.

Ashrafi et al. [42] proposed another different design of the single lap joints (Fig. 1.4c) with a sinusoidal layer of adhesive and with adherends made of fiber-reinforced epoxy composite. Experiments and finite element simulations showed that the non-flatness of the interface has important effects on the strength and on the mechanical behavior of the bonded joints; it can reduce or improve the joint strength. Haghpanah et al. [43] studied instead the importance of adhesive-adherent interface morphology on the mechanical behavior of narrow single lap joints with interlocking teeth, founding that the load bearing and the elongation at failure could be improved depending on the slope of the teeth (Fig. 1.6). The data shows that stress distribution along the bondline, as well as the initial fracture load, depends considerably by the positive and negative interlocking teeth: a crack may tend to spread or to stop depending on the morphological details. Furthermore, when crack arrests, the joint can bear a higher load and can enhance energy absorption and toughness through some of the intrinsic properties of the adherends, like the plasticity of metal adherends. Non-flattening the bonding surface is therefore a useful technique to improve the

strength of adhesively bonded joints, as well as using some interface geometries which increase the mechanical locking between the adherends. The paper of Haghpanah provided insight for the development of new multi-material and multi-component designs with properties that can be manipulated to fit for the situation, but it is limited to adhesives with brittle behavior; for the analysis of quasi-brittle behavior adhesives a non-linear fracture mechanics concept is necessary.

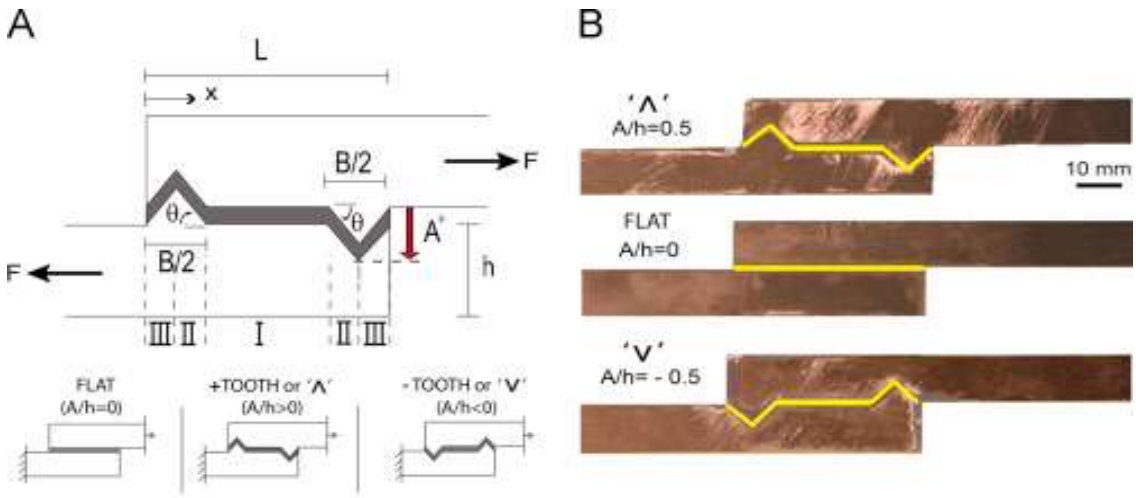

Figure 1.6. *Schematic of the bonded joint (A) and three different interface profiles (B) [43]*

In [24] some non-flat and standard single lap joints have been deeply analyzed through experimental studies and finite-element analyses on the role of the interface shape and the substrate/adhesive materials. The effects on the stress distribution and on the strength of the adhesive joint have been observed and the results show a strength improvement up to 40% compared to the conventional SLJs. According to this paper and its results, thinner bond lines, lower wave lengths and higher wave heights can considerably improve the efficiency of these lap joints. The best load-bearing improvement has been obtained with a negative bond slope and antisymmetric interface geometry, making these choices the most recommended for the zig-zag geometry and for the wavy one.

1.2 Two-dimensional and three-dimensional analyses

It is well known that an induced out-of-plane mode is generated due to Poisson's effect when cracked models are submit to in-plane shear loading. The work of Berto and Marangon in [44] recall the previous studies on the coupled mode, called mode O, in plates with sharp V-notches and different notch opening angles; in the article the negligibility of the three-dimensional effects is discussed, presenting in detail some cases of blunt V-notches, circular and elliptic holes, underlining how the three-dimensional effects are always present in those cases, even if they are negligible in some of them. This constant presence is guaranteed by the fact that mode I, mode II and mode III, the three modes of loading that are presented above, cannot exist in isolation. In its conclusions, the work of Berto and Marangon explains how the mode O is always coupled with the generating mode II loading independent of the notch shape, as well as how the intensity of this mode is linked to the Poisson's rate, disappearing when $\upsilon = 0$. This strong connection between the three-dimensional effects and the Poisson's rate, main indicator of the response along one direction to a solicitation applied on another direction, is well known and has been studied in many recent research contexts. Furthermore, another conclusion made in the above mentioned work is that the geometrical parameters of the component and the notch, like the plate thickness and the notch root radius, have a huge influence on the behaviour of the out-of-plane effects.

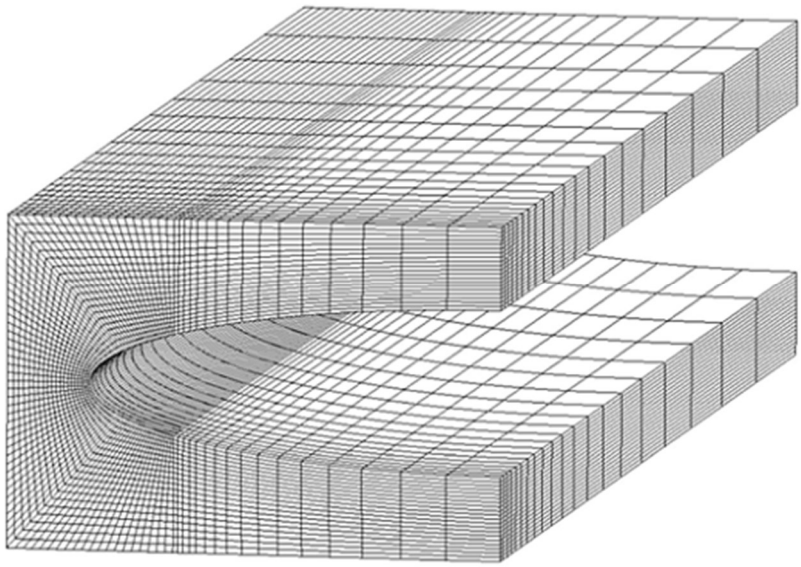

Fig. 1.7. Mesh of a b*lunt V-notch [44]*

In one of their paper [45] Richardson, Crocombe and Smith assessed the validity of modelling adhesive joints as two-dimensional problems comparing the results with the ones from three-dimensional adhesive join analyses. They proposed some modifications to the two-dimensional analyses in order to obtain results that compare favorably with their three-dimensional counterparts. This purpose was achieved by adjusting the two-dimensional loading in excess of 20%: at the time, there was a commonly accepted approach that applied an average value of load and assumed plane strain conditions, but it was noticed that this does not simulate the conditions on the mid-plane of a three-dimensional joint because the load is not transferred uniformly. The solution proposed by Richardson et al. was necessary because in 1992 a three-dimensional analysis was very challenging for the computers.

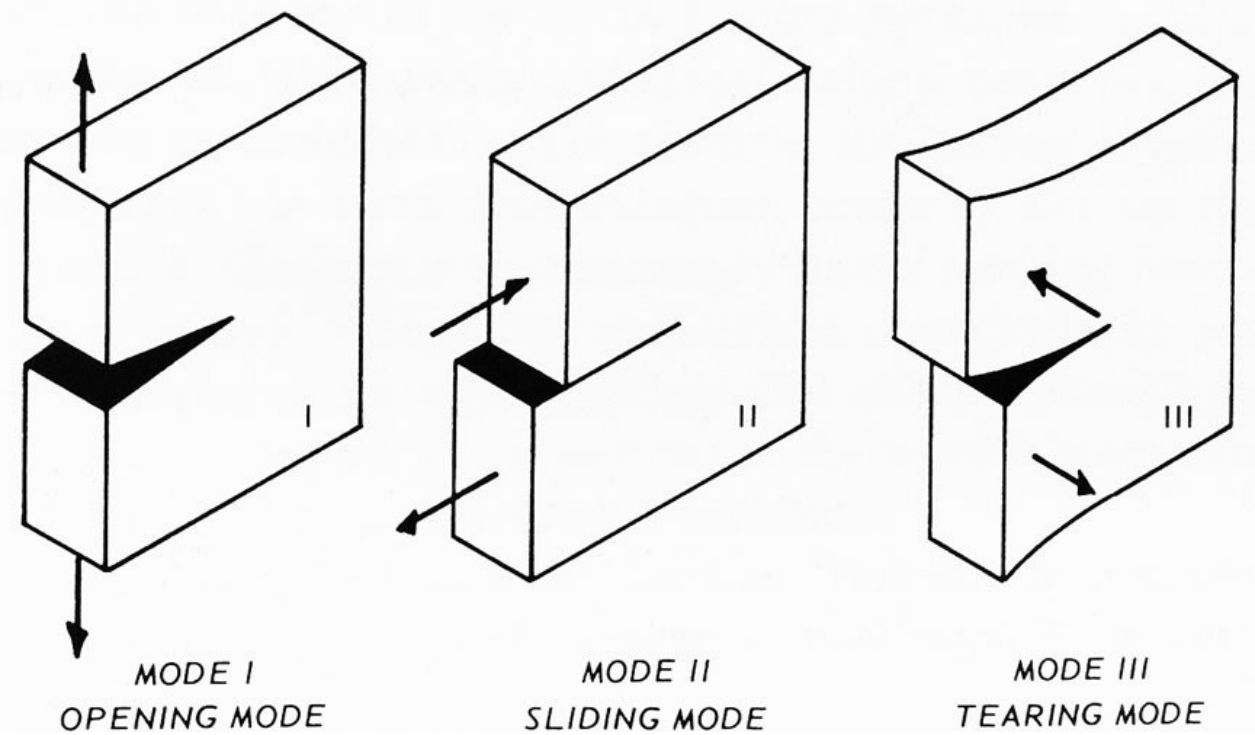

Fig. 1.7. *The three modes of loading [46]*

In [46] Ewalds and Wanhill explain the nature of the three fundamental modes of loading in the vicinity of a crack tip, as shown in Fig. 1.7, which are the opening mode, the sliding mode and the tearing mode. The first two operate within the plain and should create an in-plane stress distribution, on the contrary the last one operates on the third direction; every mode operates in a different manner but all of them contribute to the failure of the crack. The combination of more than one mode at the same time creates the so called "mixed mode", more challenging in terms of complexity and damage.

The out-of-plane effects are so important in the field of adhesively bonded joints because, even if the joint undergoes an in-plane stress applied by an external factor, its physicality gives life to a three-dimensional stress distribution. Normally the crack represented by the corner of the joint is submitted to a mode one stress, or at least that is the predominant situation in many practical cases; however, this condition leads to a compression of the material along the out-of-plane direction which creates a mixed mode of solicitation, a three-dimensional one. This particular mixed mode is complex and hard to be predicted, it depends by the geometry of the model and by the nature of the material and both of these aspects require deep investigations; a three-dimensional analysis is fundamental to fully understand this topic, making the research even more difficult.

As it is fully explained in the paper of Afshar et al. [47], almost all analytical models for adhesively bonded lap joints are two-dimensional and does not consider the out-of-plane stresses. For example, the extensive review presented in [48] and [49] compares the previous analytical models for both single and double lap joints pointing out that it is not necessary to introduce the stresses in the width direction because they are significantly lower than the ones in the other directions. Instead the work of Bogdanovich et al. [50] used a three-dimensional finite element analysis with submodeling approach to deeply verify double-lap composite adhesive bonded joints exposed to uniaxial extension. The main objectives were to explore the advantages of the multi-step submodeling approach and to perform one of the first comprehensive numerical study of three-dimensional joint structures, where the adhesive layer were considered as 3D elastic entities. The analysis had some problems related to the huge number of elements and was not able to obtain a full stress distribution in the critical zone, neat the ends of the overlap, and it was extended with a numerical study performed with a two-dimensional plane stress formulation.

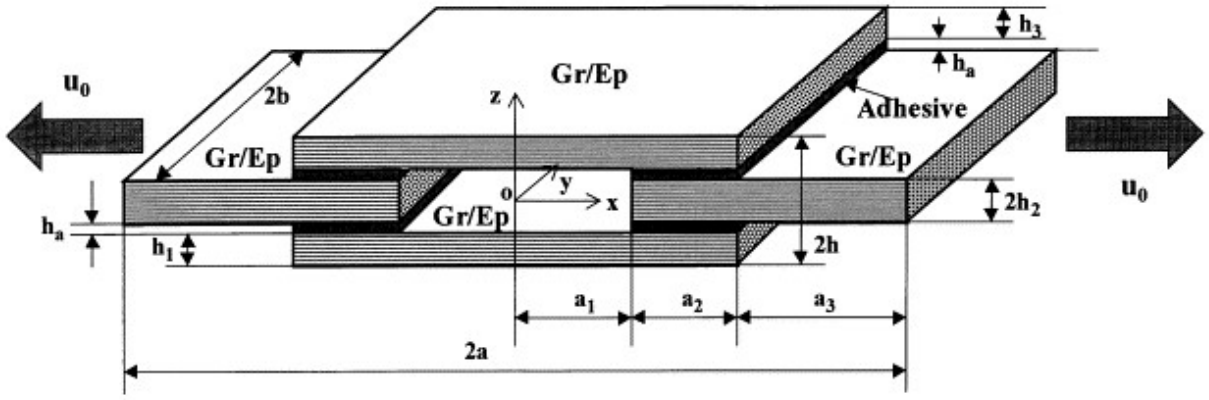

Fig. 1.8. *Double-lap adhesive bonded joint [50]*

The work of Afshar, Berto and Lazzarin [47] analyzes the three-dimensional elastic stress distributions in the proximity of adhesive's layer corners, where the higher stress concentration can be found. The aim was to show the effects of the adhesive thickness and the Poisson's ratio variations on the out-of-plane shear stress distribution in these highly stressed regions.

The work of Gonçalves et al. [51] is another proof of how risky it is to underestimate the out-of-plane stresses using a two-dimensional analysis: they presented a new model for three-dimensional finite element analysis of adhesive joints that considers both geometric and material nonlinearities. Their results highlighted the three-dimensional nature of the stress concentrations and stresses in the proximity of the interface, as it is clear from the geometry of Fig. 1.9 and the graphics of Fig. 1.10. This is the reason why they strongly suggested to be very careful in using the bi-dimensional models in the strength prediction of adhesive joints; it was also observed that the peak stresses are much higher at the interfaces than the ones in the middle of the adhesive layer, confirming the reason why the interfaces are critical zones for the failure of adhesive joints.

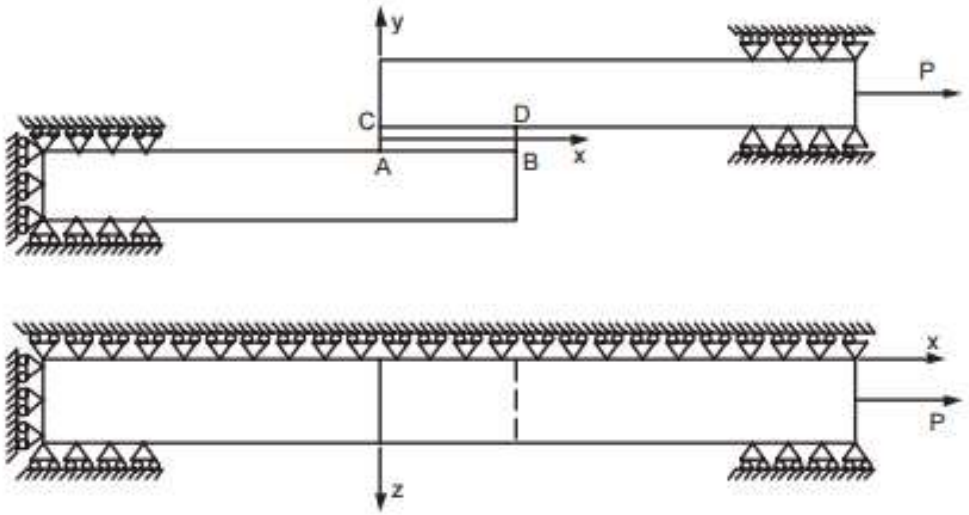

Fig. 1.9. *Geometry and boundary conditions of Gonçalves' model [51]*

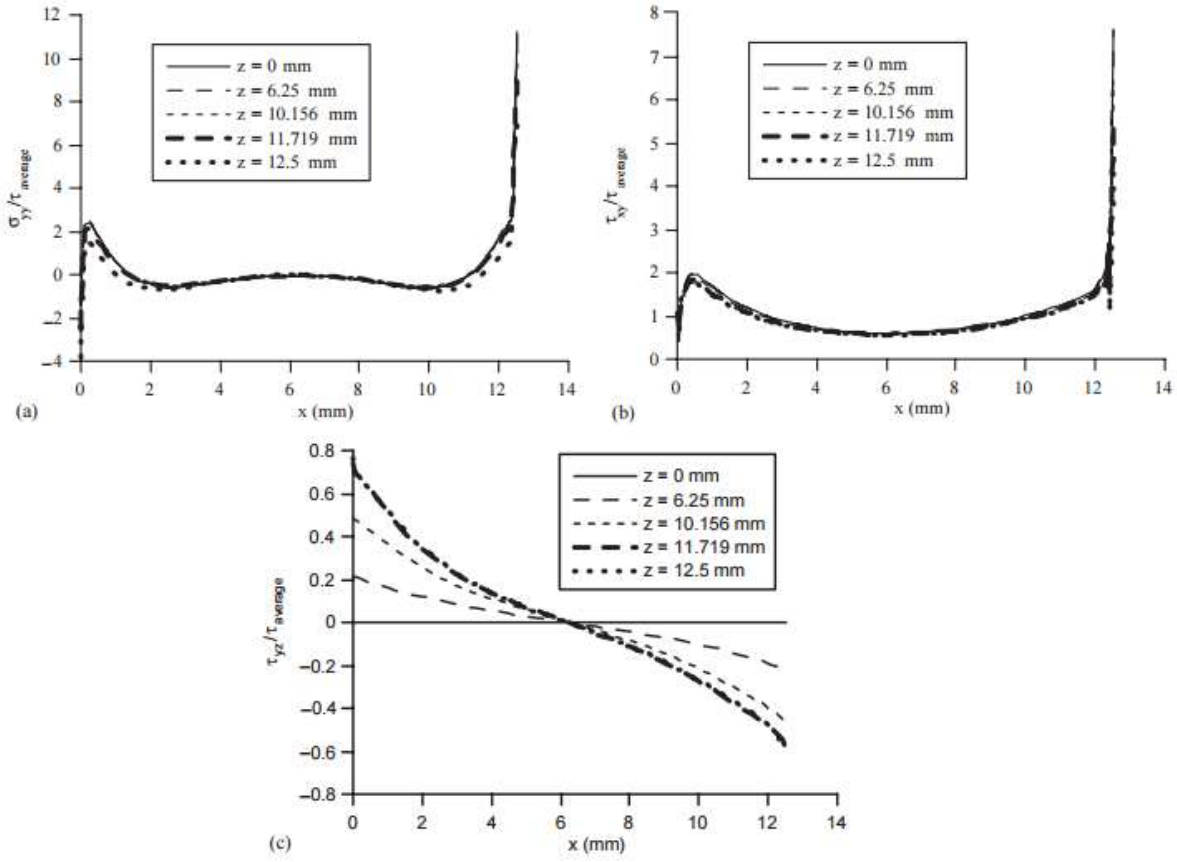

Fig. 1.10. *(a) Normalized stress σ_{yy} at the interface. (b) Normalized stress τ_{xy} at the interface. (c) Normalized stress τ_{yz} at the interface [51]*

3D finite element viscoplastic analysis with geometric nonlinearity of lap joint was studied by Narasimhan [52] and Pandey et al. [53, 54], while Tsai and Morton [55] focused on the 3D study of a single lap joint in a linear elastic finite element analysis where the geometrically nonlinear effects were represented by the boundary conditions. They confirmed the existence of a 3D region in which adherent and adhesive stress distributions along the overlap length near the surface were significantly different from those of the interior; furthermore, the adhesive peel stress seemed to be very sensitive to 3D effects. The maximum value for the peel stress occurred in the proximity of the end of the overlap in the central two-dimensional core region, rather than at the corners where the 3D effects were found. From these consideration, in 2001 another article from Pandey et al. [56] was written: it compared two- and three-dimensional finite element analysis on single lap joints, plotting the peel and shear stress along the width and noticing different behaviours in different locations. At the edges the peel stress values were close to plane strain, with a 5% distance from the 2D values on the ends of lateral width; the shear stress the behaviour was visibly 3D in all the considered cases. At the center, there was a clear enhanced three-dimensional behavior throughout the width, but its magnitude was not significantly different from 2D value. In the other places, the peel distributions also showed differences between the 3D regions and the plane strain locations. From the observations made on the identifications of three-dimensional zones, Pandey concluded that 3D analysis gives significantly different stress distributions away from the central region and underline the need for three-dimensional analysis in the works regarding behavioral study and joint design. However, despite this, only in the last years some works like the one of Akpinar et al. [12] or the one of Doru et al. [18] started analyzing 3D stress distributions instead of the simpler 2D model. This needs for sure a bigger effort that is not always required, but sometimes it is necessary to consider the three-dimensional effects because of their magnitude.

In [57] Campagnolo et al. underline once again that even if the understanding of three-dimensional effects is constantly increasing, these phenomena are sometimes not considered in contexts where they could be very significant. The study carried out by Campagnolo, Berto and Pook reviewed some other works of the same authors that investigated a coupled fracture mode generated by anti-plane loading of a straight through-the-thickness crack in elastic plates and discs, analyzed thanks to accurate three-dimensional finite element models. The evaluation of local stress

and strain state along the thickness of the geometry had been made using the strain energy density (SED) averaged in a determined control volume surrounding the crack tip (Fig. 1.11).

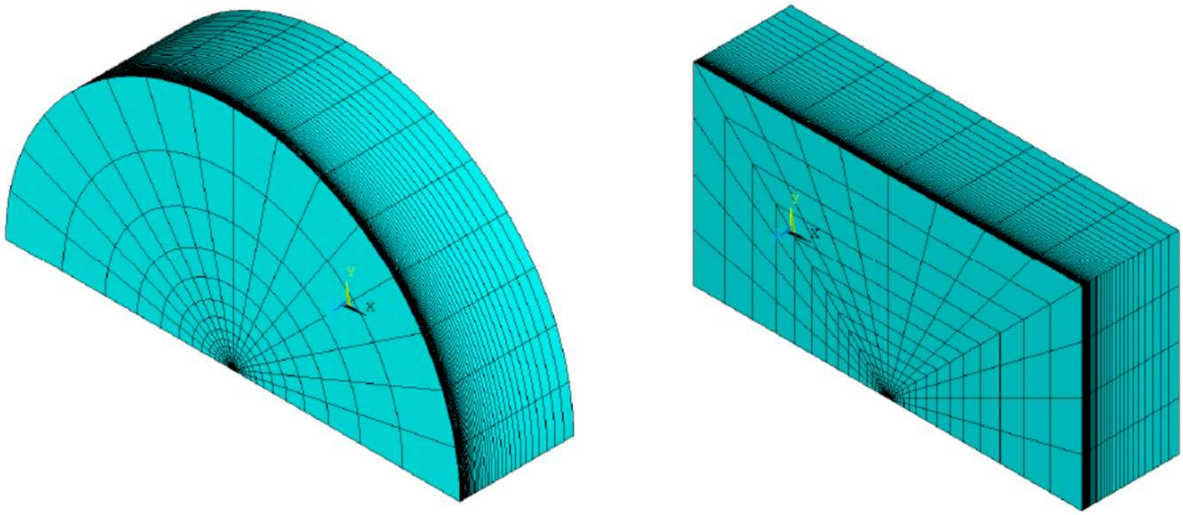

Fig. 1.11. *Overall view of FE meshes: (a) disc and (b) plate [51]*

The results of the highly accurate FE analyses improved the knowledge of anti-plane loading behavior in cracked discs and plates: it was proved that the influence of plate bending increases its importance when the thickness decreases; the anti-plane nominal mode III loading has been used and the fact that mixed modes III and II loading are impossible to separate from each at other, at the present state-of-the-art, has been confirmed and underlined. This work tried to complete other previous studies on the symmetric mode (mode I) made by other authors, but in the end it reports that the theoretical understanding of the stress field in the proximity of a corner point is still far from being complete.

From this short review of the previous papers regarding the topic of adhesively bounded joints it is easy to understand the importance of keeping on with the analysis of different cases, especially with three-dimensional geometries. This is the reason that has begun this paper, to deepen the topic without the claim to be fully exhaustive.

Chapter 2

Finite element method

This chapter shortly introduces the finite element method and explains the choices made during the pre-analysis phase, presenting the geometric model with boundary conditions, elements, mesh and strategy adopted for modeling the joint. Furthermore, a short review on the meaning of K_i values and on how to obtain them is presented.

2.1 Geometric model

A 3D model of a single-lap wavy joint with dimensions given in Fig. 2.1-2.2 was considered to study the intensity of the in-plane and out-of-plane stress distributions with linear elastic behaviour assumption. Due to the symmetry of the model along the width, only half of the joint was considered making the analysis much simpler and faster; the geometry of the joint has been designed to avoid any bending moment that could appear if the dimensions and the stresses applied to the sample had not been properly studied.

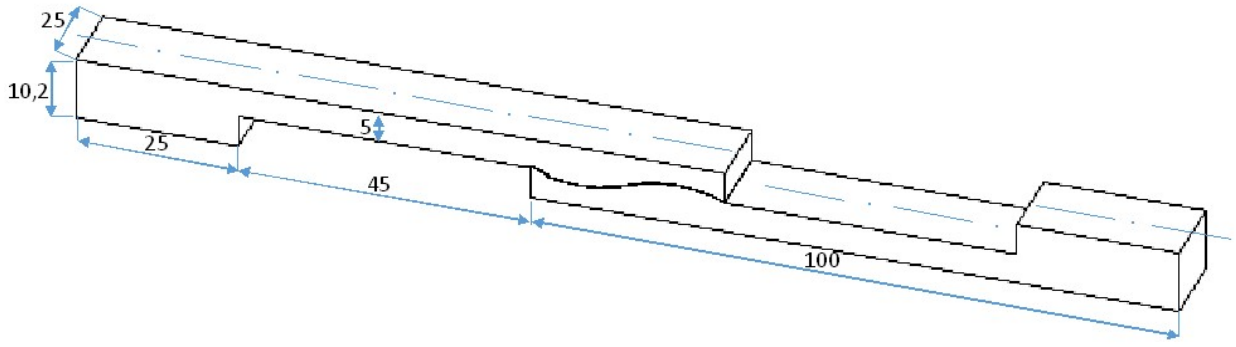

Fig. 2.1. *3D view of a single-lap wavy joint (A<0, Nwaves=2)*

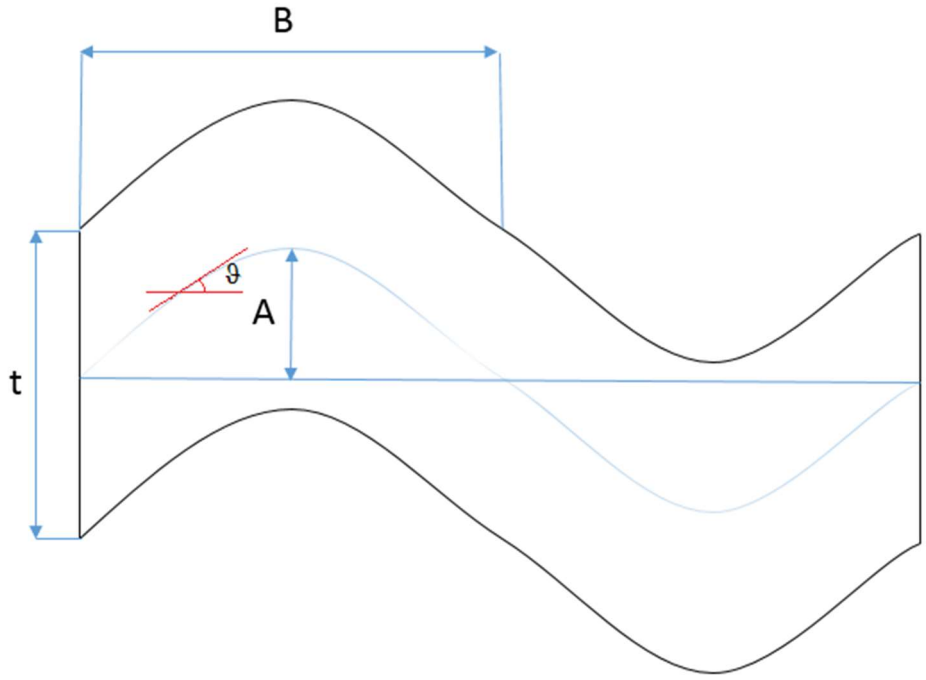

Fig. 2.2. *Geometry of the layer (A>0, Nwaves=2)*

The following formula describes the function which was used to draw the contour of the sinusoidal layer:

$$y_n = A\ sen\ (\frac{\pi}{B} x_n) \qquad (2.1)$$

where x_n and y_n are the coordinates of the n-th keypoint and y_0 is the y coordinate of the joint's left corner, A is the height of the wave and B is its length.

Fig. 2.3 illustrates the boundary conditions and the loads: the joint is bonded by a build-in support on the left and by a simple support on the left. Furthermore, the Y-translations of the nodes on the right surface have been forced to be all equal, making it possible for that surface to translate rigidly without any rotation.

Fig. 2.3. *Mesh pattern and boundary conditions*

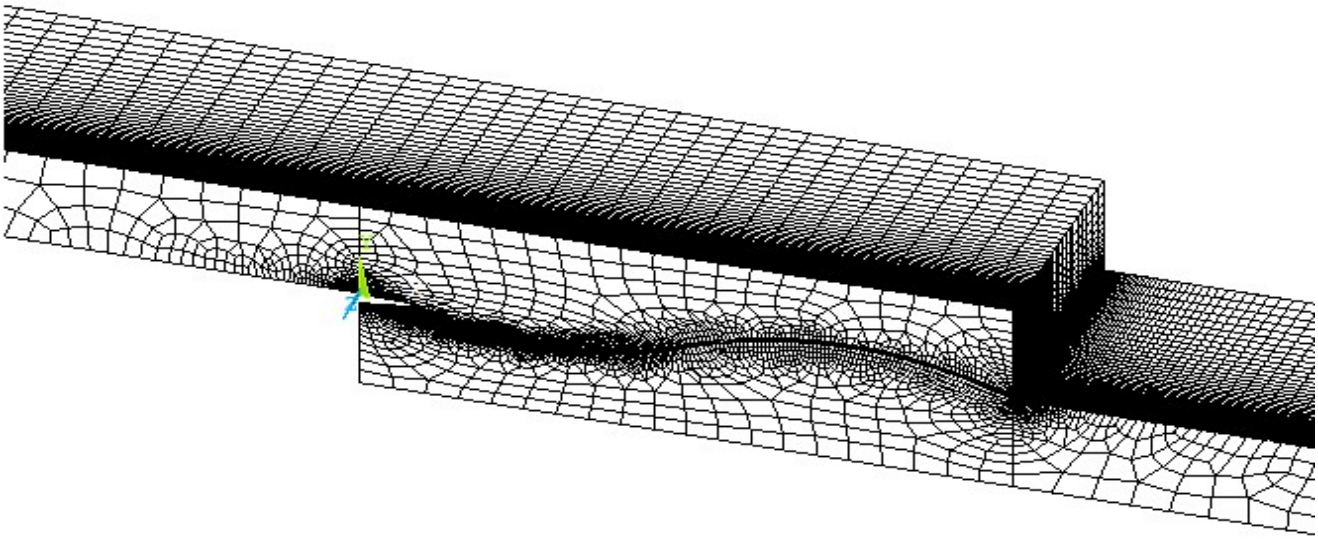

Fig. 2.4. *Global mesh*

A Young's modulus of E = 70 GPa and a Poisson's ratio of ν = 0.33 were initially employed in numerical analysis for the aluminum; the adhesive was characterized by a Young's modulus of E = 2 GPa and a Poisson's ratio of ν = 0.33 instead.

First, the mesh of the surface has been realized using a 4-node quad element 182 focusing especially on the left corner of the joint, the more stressed one, and building an appropriate scheme

of lines to have the desired refined mesh only where it was necessary. After finishing the surface mesh, a line along the width of the joint has been created and divided in order to extrude the mesh and turn it into a three-dimensional one.

The 8-node brick hexaedral elements 185 were used to mesh the final finite element model everywhere but in the zone where the concentrate keypoints had been used. As illustrated in Fig. 5a, higher mesh density was used near the left corner of the adhesive, up to a minimum size of $4x10^{-4}$ mm. Besides, 6-node prismatic elements were used for the first ring of elements around the edge (Fig. 2.5b): these elements could be less accurate than the hexaedral ones, but they are necessary in order to obtain a clear mesh.

The number of waves has been used as a parameter, making it change from 2 to 6, as well as their height; the distance from the left corner of the joint is another fundamental factor that helps in finding the K_i values as illustrated in the next section.

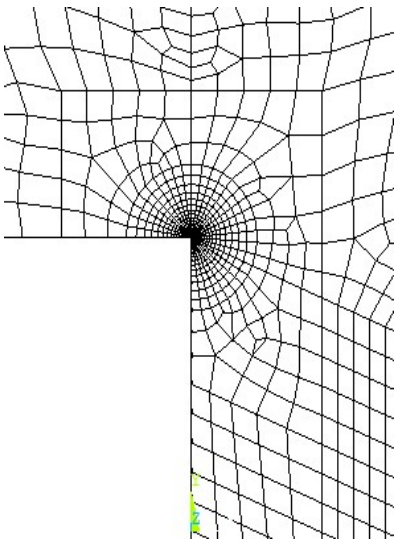

Fig. 2.5a. *Overlap corner*

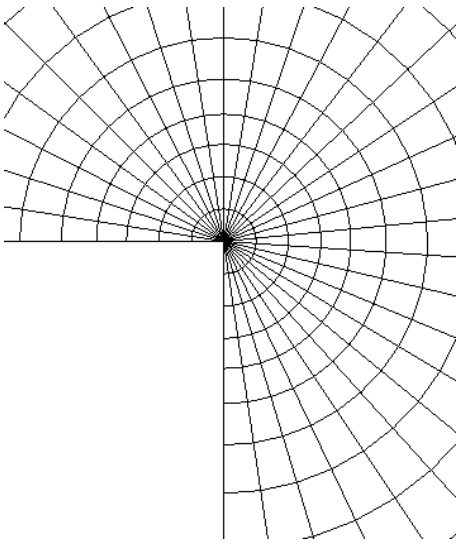

Fig. 2.5b. *Focus on the corner*

One of the trickiest tasks during the modeling has been the realization of the mesh, which supposed to be very dense around the corner (Fig. 2.5b) and on the surface because of the geometric singularity; on the other hand, too many three-dimensional elements would have compromised the resolution speed, if not blocking the program at all. Those are the reasons that

explain the mesh in Fig. 2.4, with a huge difference between the dimensions of elements on the surface and in the core of the joint. Along all the adhesive layer a quite thick mesh has been used because of its thinness and the material discontinuity, using less elements could have brought to some numerical errors.

2.2 Analytical model

Five different paths (Fig. 5) have been chosen to obtain the K_1^{App}, K_2^{App} and K_3^{App} factors starting from the values of $\sigma_{\vartheta\vartheta}$, $\tau_{\vartheta r}$ and $\tau_{\vartheta z}$. The main aim was to verify where the A-NSIFs were stable along the length to study, in a second time, the same values on a new path along the width.

$$K_1^{App} = \lim_{r\to 0} \sqrt{2\pi}\, r^{\xi 1} \sigma_n \qquad (2.2)$$

$$K_2^{App} = \lim_{r\to 0} \sqrt{2\pi}\, r^{\xi 2} \tau_{s2} \qquad (2.3)$$

$$K_3^{App} = \lim_{r\to 0} \sqrt{2\pi}\, r^{\xi 3} \tau_{s3} \qquad (2.4)$$

These are the formulations presented by Gross and Mendelson [54] for a plane elastostatic analysis of V-notched plates but in this work they are applicated to the corner of a three-dimensional joint, which is directly comparable to a V-notch; this appears clearly legit when watching at the corner as a notch with a 90 degrees angle.

To calculate the K_i^{App} values the in-plane and out-of-plane stresses are necessary: σ_n, τ_{s2} and τ_{s3} are respectively the in-plane stress orthogonal to the layer, the in-plane stress tangential to the layer and the out-of-plane stress tangential to the layer. The numerical simulation provides an estimate of the stress distribution in the joint, giving σ_{xx}, σ_{yy}, σ_{zz}, τ_{xy}, τ_{xz} and τ_{yz}; these data were used to obtain the peel and shear stresses according to:

$$\sigma_n = \sigma_{xx} \sin^2\vartheta + \sigma_{yy} \cos^2\vartheta - 2\sigma_{xy} \sin\vartheta \cos\vartheta \qquad (2.5)$$

$$\tau_{s2} = -(\sigma_{xx} - \sigma_{yy}) \sin\vartheta \cos\vartheta + \sigma_{xy} (\cos^2\vartheta - \sin^2\vartheta) \qquad (2.6)$$

$$\tau_{s2} = (\sigma_{zz} - \sigma_{yy}) \sin\vartheta \cos\vartheta + \sigma_{yz} (\cos^2\vartheta - \sin^2\vartheta) \qquad (2.7)$$

where ϑ is the angle formed by the adhesive layer and the x axis at a given section, as previously shown in Fig. 2.2 (where ϑ=0 symbolize a flat joint). The geometrical values ϑ and r, the distance from the corner used in the next analysis of the results, were calculated from the coordinates of every node with the following simple expressions:

$$\vartheta_n = \pi \frac{A}{B} cos\left(\frac{\pi}{B} x_n\right) \qquad (2.8)$$

$$r_n = \sqrt{{x_n}^2 + (y_n - y_0)^2} \qquad (2.9)$$

where x_n and y_n are the coordinates of the n-th keypoint and y_0 is the y coordinate of the joint's left corner. The formula 2.8 has been obtain by the derivation of the function which describes the geometry of the layer to be sure that the angle will always be tangential to that line. This process must be repeated five times per model, one time for each of the five paths in Fig. 2.6, to verify if there is a certain distance from the core of the mesh in which the K_i values can be considered constant and how this distance varies along the width of the joint.

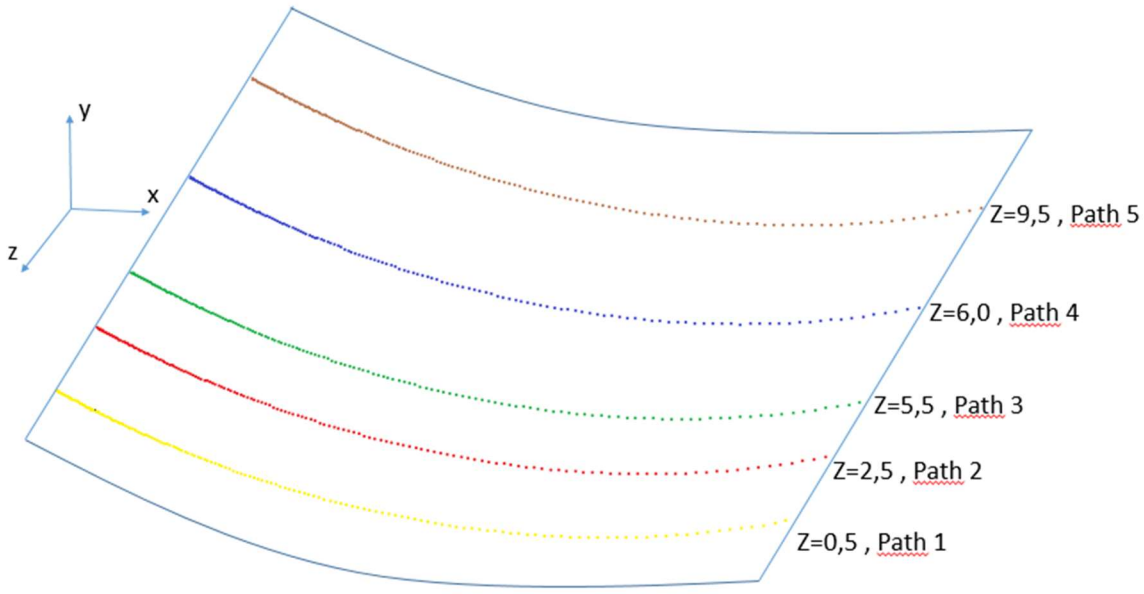

Fig. 2.6. *Paths projected on the surface of the adhesive layer*

The position of the different paths is important because of the singularities presented in the previous section and in other works like the one of Afshar, Berto and Lazzarin [47] where different values of K_1^{app} and K_3^{app} have been calculated and plotted together for three different geometries of the layer (h_{adh} = 0.10, 0.25, 0.50). Fig. 2.7 shows how the K_i values are about constant close to the lateral surface, between 4.5 and 4.95 mm from the surface, but they tend to increase considerably when getting too close to it. All the three stress components σ_n, τ_{s2} and τ_{s3} were singular and the peel stress was the maximum one.

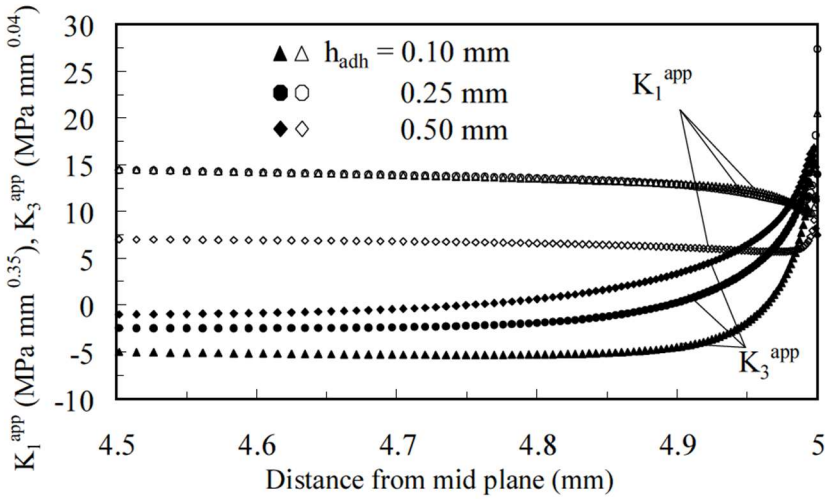

Fig. 2.7. *K_1^{app} and K_3^{app} distributions along the width of a SLJ [47]*

Being the mesh used by Afshar et al. much finer than the one of this analysis, it can be utilized as a good comparison term for the post-results discussion; furthermore, that paper investigated the influence of the layer thickness and Poisson coefficient while this thesis focuses on the height and the length of a wavy interface: the two works can be used together to have a more complete point of view.

Chapter 3

Results and discussion

This chapter illustrates the results obtained with the FE analyses and the reasoning behind the choices made during this phase of the study, as well as the differences between the analyses of the wave length, of the wave height, of the layer's thickness and of the adherent's elastic modulus. Some important considerations about the trends of the data are made, giving a reasonable interpretation of the stresses distributions.

3.1 First parameter: wave length

The first part of the joint analysis gives the stress distribution along the paths described before for every different geometry connected to the length of the waves (NW from 2 to 6), comparing them with the ones of the flat joint; this results can be easily turned into the A-NSIF values K_1^{App}, K_2^{App} and K_3^{App} after obtaining the singularity degree ξ from the slope of the double logarithmic graph σ_i/r, as shown in Fig. 3.1.

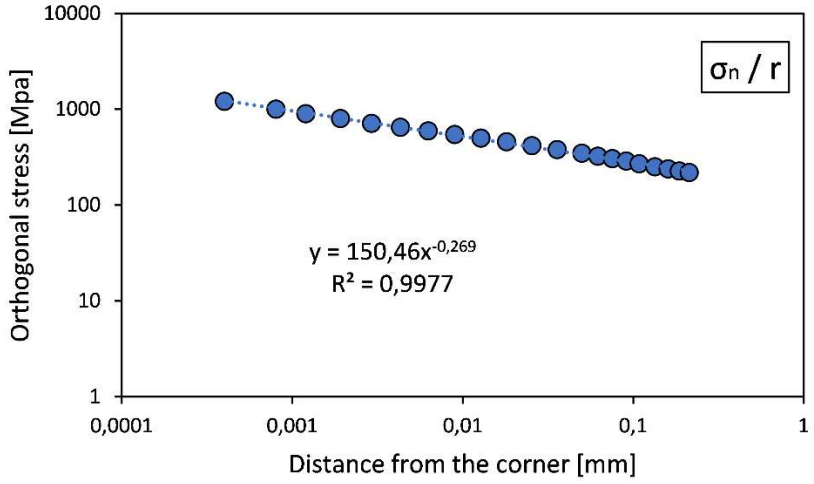

Fig. 3.1. *Double logarithmic graph σ_n/r for path 1 (NW=2, A=-1.5)*

All the graphics that illustrates the stress distribution of σ_n, τ_{s2} or τ_{s3}, like the ones in Fig 3.2 - 3.3, underline the same pattern when using the double logarithmic scale for the axes, regardless of which number of waves has been used during the modeling. The linear relation between the two logarithmic values is clear, with a R^2 coefficient which is almost unitary.

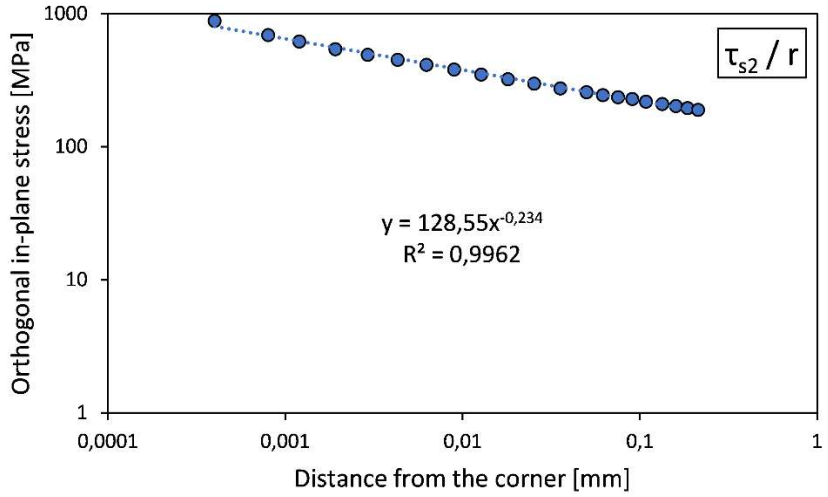

Fig. 3.2. *Double logarithmic graph τ_{s2}/r for path 1 (NW=2, A=-1.5)*

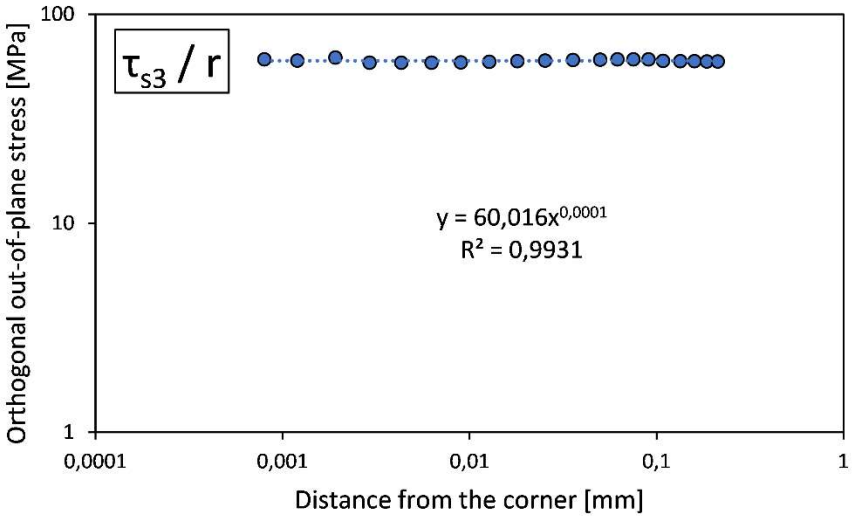

Fig. 3.3. *Double logarithmic graph τ_{s3}/r for path 1 (NW=2, A=-1.5)*

Figures from 3.4 to 3.6 well represent the second step of the data elaboration: starting from the degrees of singularity obtained before, it is possible to calculate the apparent generalized notch stress intensity factors for every geometry and path. These values result to be almost constant along the length of the joint.

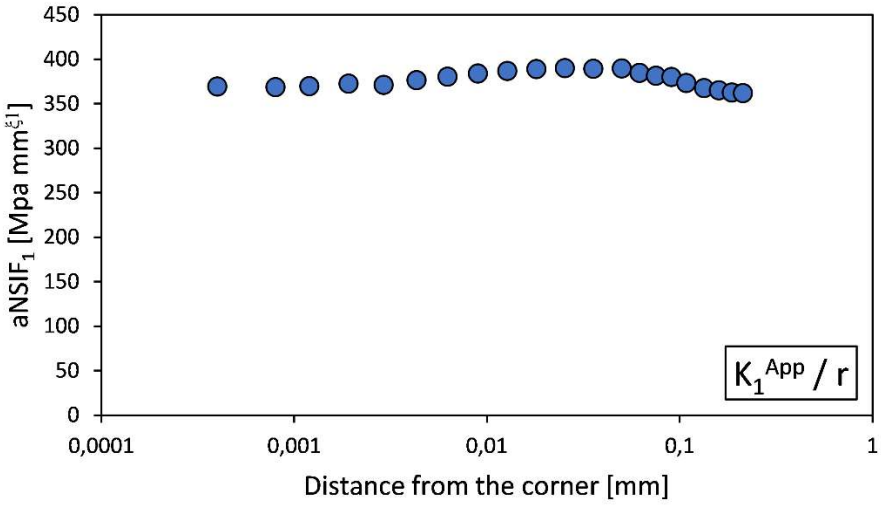

Fig. 3.4. *Logarithmic graph K_1^{App}/r for path 1 (NW=2, A=-1.5)*

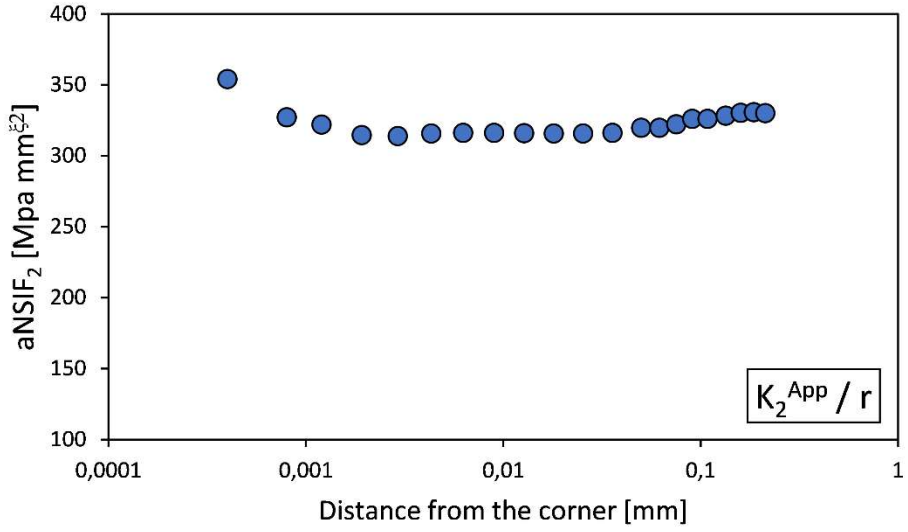

Fig. 3.5. *Logarithmic graph K_2^{App}/r for path 1 (NW=2, A=-1.5)*

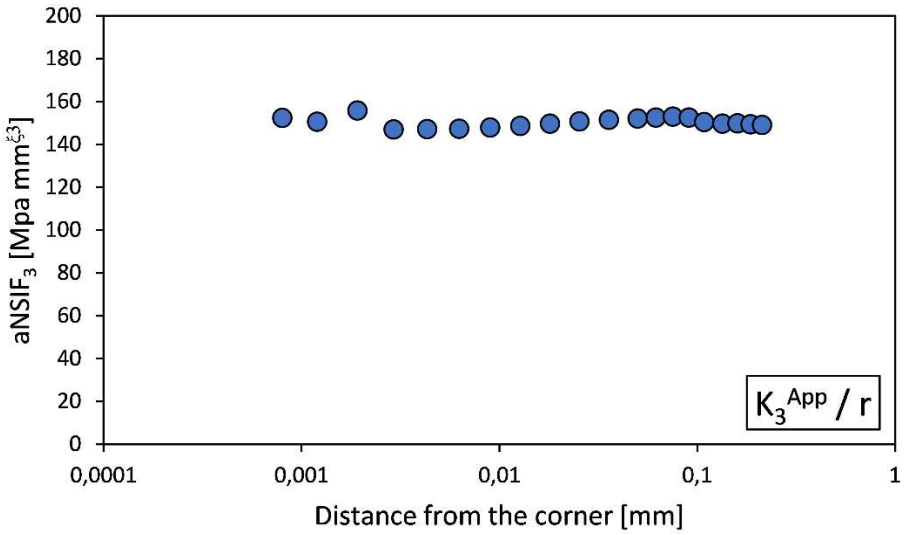

Fig. 3.6. *Logarithmic graph K_3^{App}/r for path 1 (NW=2, A=-1.5)*

The trends of these values are quite satisfactory and they respect the expectations which preceded this work: the K_i^{App} values can be considered constant in a certain range of distance from the left corner of the joint without introducing a big approximation, all the graph reported before are a clear confirmation of this statement. It is a result in line with the previous studies carried out on this topic, giving it a certain degree of reliability and allowing the continuation of the analysis.

The following tables, from Tab. 3.1 to 3.5, report the values of K_i^{App} for different number of waves: as mentioned before, all these values appear to be constant when moving from the left corner to the opposite one. Furthermore, different geometries share the same pattern when moving from a path to another, but this fact will be more evident from the summary graphs that are reported below.

The degree of singularity reported in the tables tend to be steady even along the width direction, except for the first paths (the closest to the lateral surface) that are different from the others because of the vicinity to the singularity.

Path	z [mm]	ξ_1	K_I^{App}	ξ_2	K_{II}^{App}	ξ_3	K_{III}^{App}
1	0,5	0,269	376,83	0,234	322,72	0,0001	150,34
2	2,5	0,256	464,63	0,242	330,42	0,0260	108,41
3	5,5	0,252	508,97	0,244	340,18	0,0400	74,30
4	6	0,252	522,32	0,244	346,47	0,0490	53,58
5	9,5	0,252	526,59	0,244	349,02	0,0550	42,77

Tab. 3.1. *A-NSIF results along the paths (NW=2, A=-1.5mm, t=0.20mm)*

Path	z [mm]	ξ_1	K_I^{App}	ξ_2	K_{II}^{App}	ξ_3	K_{III}^{App}
1	0,5	0,303	501,35	0,314	211,21	0,069	186,47
2	2,5	0,291	597,73	0,324	213,18	0,088	146,11
3	5,5	0,287	646,31	0,328	216,33	0,098	118,40
4	6	0,287	661,42	0,328	219,93	0,104	101,73
5	9,5	0,286	656,05	0,328	221,46	0,108	92,90

Tab. 3.2. *A-NSIF results along the paths (NW=3, A=-1.5mm, t=0.20mm)*

Path	z [mm]	ξ_1	K_I^{App}	ξ_2	K_{II}^{App}	ξ_3	K_{III}^{App}
1	0,5	0,359	483,01	0,398	58,71	0,184	184,32
2	2,5	0,347	576,09	0,442	48,35	0,203	156,32
3	5,5	0,343	620,65	0,465	43,73	0,214	140,92
4	6	0,342	637,03	0,471	42,97	0,222	130,87
5	9,5	0,342	641,87	0,471	43,20	0,226	125,93

Tab. 3.3. *A-NSIF results along the paths (NW=4, A=-1.5mm, t=0.20mm)*

Path	z [mm]	ξ_1	K_I^{App}	ξ_2	K_{II}^{App}	ξ_3	K_{III}^{App}
1	0,5	0,402	410,88	0,401	58,15	0,279	161,24
2	2,5	0,391	486,27	0,359	84,55	0,296	147,20
3	5,5	0,388	522,11	0,344	98,07	0,303	144,01
4	6	0,387	535,78	0,341	102,10	0,307	141,50
5	9,5	0,387	539,77	0,340	103,37	0,311	139,11

Tab. 3.4. *A-NSIF results along the paths (NW=5, A=-1.5mm, t=0.20mm)*

Path	z [mm]	ξ_1	K_I^{App}	ξ_2	K_{II}^{App}	ξ_3	K_{III}^{App}
1	0,5	0,441	271,92	0,448	121,39	0,351	119,59
2	2,5	0,429	331,65	0,428	155,64	0,359	121,76
3	5,5	0,425	358,82	0,420	172,42	0,359	129,54
4	6	0,424	368,37	0,419	177,32	0,360	134,33
5	9,5	0,423	372,64	0,419	178,65	0,362	133,45

Tab. 3.5. *A-NSIF results along the paths (NW=6, A=-1.5mm, t=0.20mm)*

The tables above show that the K_i^{App} values vary between very different numbers when considering a variable number of waves, so it is useful to spend some more lines on their nature trying to find their trend.

The following graphics, from Fig. 3.7 to Fig. 3.9, are the most representative of this first part of the work: they represent the patterns K_1^{App}, K_2^{App} and K_3^{App} in function of the five paths for every different number of waves; the graphs from Fig 3.10 to Fig. 3.12 show instead the a-NSIF values in function of the number of waves, reversing the point of view. In both cases the values regarding a flat joint analysis with the same joint length, width and layer's thickness is represented to have a comparison term for a more complete review.

In Fig. 3.7 K_1^{App} has a clear pattern that goes down to the values of NW=6, with the only exception of NW=2 that is in the middle of the others. Increasing the number of waves seems to reduce the apparent generalized notch stress intensity factor from a maximum of 700 to a minimum of 330 when considering the fourth and the fifth paths; it would be interesting to see what would happen when the number of waves is even higher, but with this geometry it is not possible to do that: it would require a different mesh and the machining to make the joint could result more difficult. The flat joint's values are the lowest in this case, even lower than the ones corresponding to the number of waves equal to six.

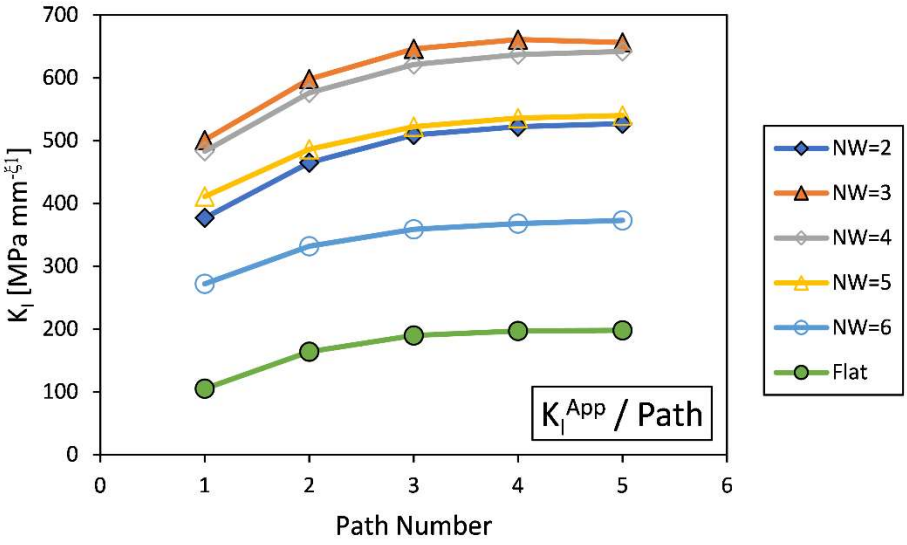

Fig. 3.7. *Graph of K_I^{App} in function of the paths for different numbers of waves (A=-1.5)*

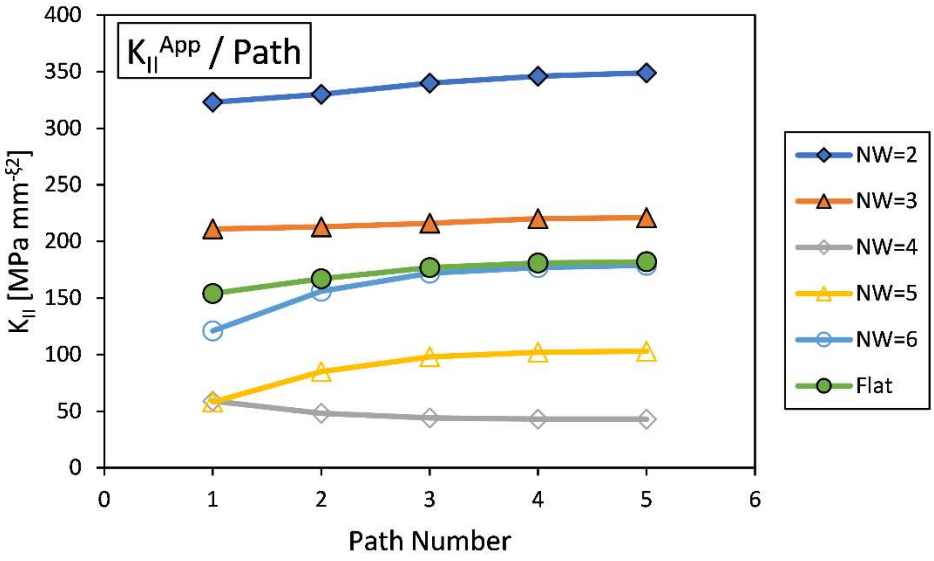

Fig. 3.8. *Graph of K_{II}^{App} in function of the paths for different numbers of waves (A=-1.5)*

Fig. 3.8 show a different trend compared to the previous one: in fact, the lowest values for K_2^{App} have been obtained with the four waves geometry while the values of the reference flat joint stay in the middle. It seems that this a-NSIF value tends to decrease when increasing the number of waves, but with NW=4 it reaches its minimum; further increasing the number of waves leads to a new rise of K_2^{App}, first with NW=5 and then with NW=6.

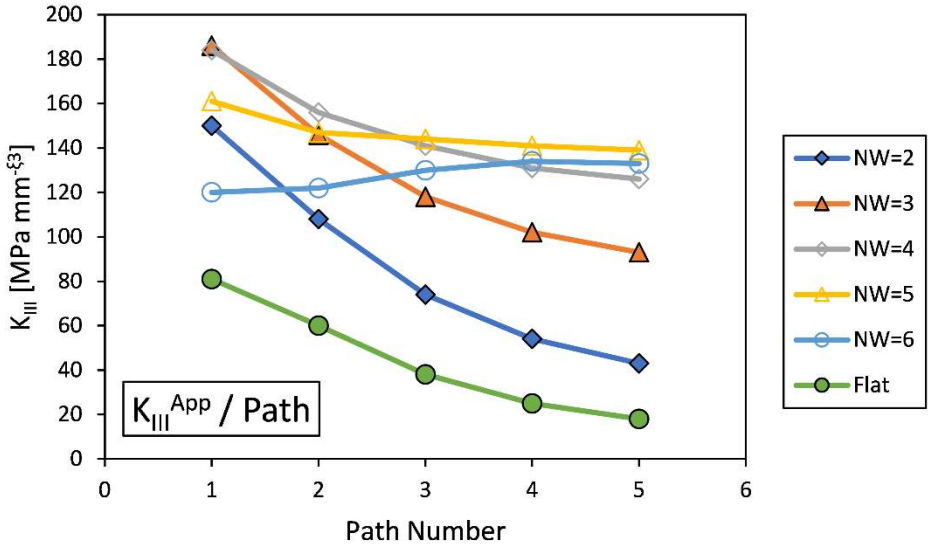

Fig. 3.9. *Graph of K_{III}^{App} in function of the paths for different numbers of waves (A=-1.5)*

The last graph (Fig. 3.9) of this series seems to be more complicated than the others: for the first two paths, it shows a pattern which is similar to the one of Fig. 3.7, with lower values of K_3^{App} for higher values of NW; moving into the width, through paths 3, 4 and 5, inverts this trend and gives the highest values of K_3^{App} for the lowest number of waves. Another interesting observation that can be made on this graph is that even the trend of K_3^{App} in every single model changes: for the lower number of waves K_3^{App} decreases when moving along the width from the first path to the last one; for NW=5 the value is almost constant; for NW=6 instead the trend is the opposite and the apparent generalized notch stress intensity factor increases from the lateral surface to the middle of the joint.

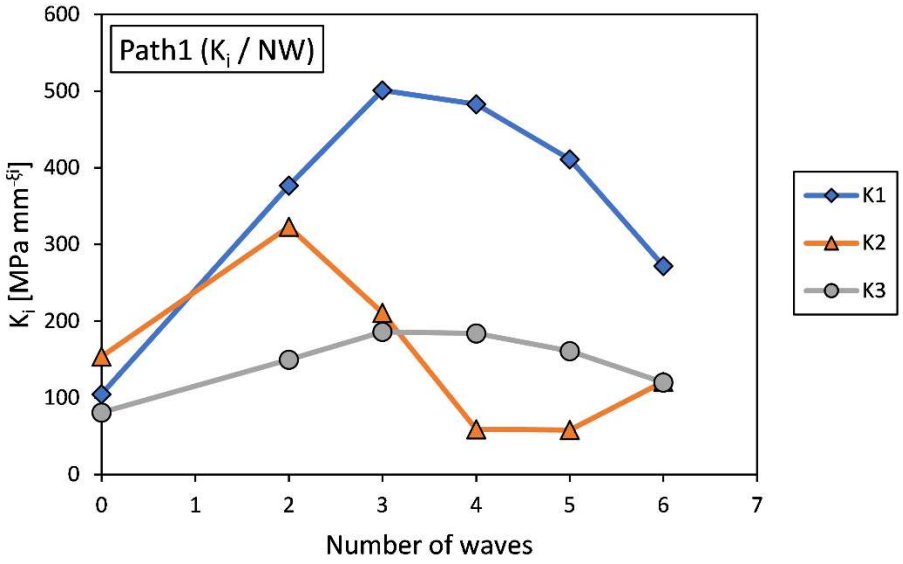

Fig. 3.10. *Graph of K_i^{App} in function of the number of waves for path 1 (A=-1.5)*

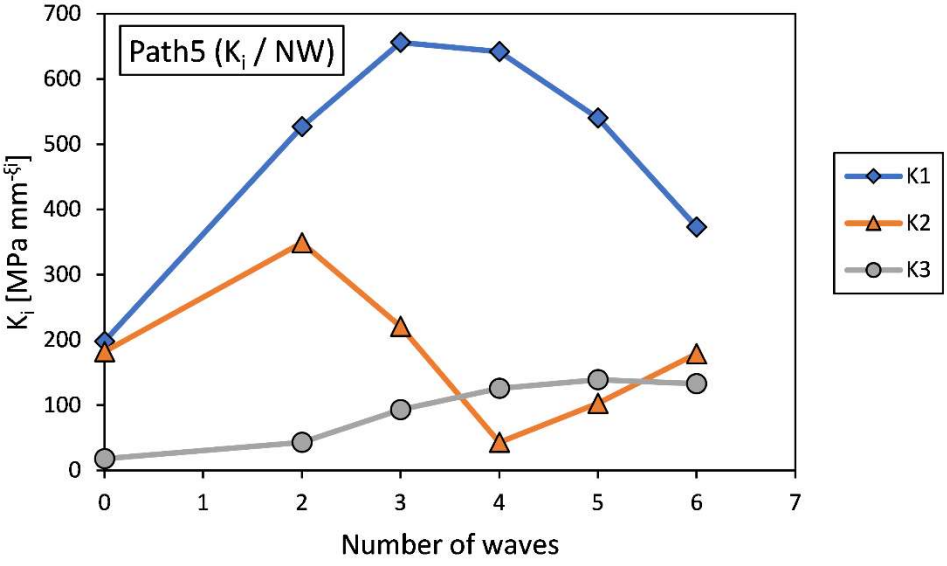

Fig. 3.11. *Graph of K_i^{App} in function of the number of waves for path 5 (A=-1.5)*

The last two graphs, Fig. 3.10 and 3.11, represent the variation of K_i^{App} in function of the number of waves for the first and the fifth path; the remaining paths are not reported because they share the same trend with these two. Once again, the data characterized by NW=0 are the one corresponding to the flat joint which clearly contains no waves. As mentioned above, the apparent generalized notch stress intensity factors follow different ways: K_1^{App} initially increases when increasing the number of waves and invert this tendency after NW=3; K_2^{App} has an opposite behaviour, showing a minimum for NW=4; lastly, K_3^{App} follow the conduct of K_1^{App}, although it is slower.

3.2 Second parameter: wave height

The second part of the analysis is similar to the first one but it considers instead sinusoidal wavy interfaces with different heights and not with different wave lengths. This time it has been chosen a number of waves equal to two and, once again, a thickness equal to 0.2 mm; the height has been changed from -0.5 to -3.0 and the results have been confronted with the flat joint (A = 0).

Path	z	ξ_1	K_I^{App}	ξ_2	K_{II}^{App}	ξ_3	K_{III}^{App}
1	0,5	0,361	159,25	0,163	273,28	0,059	90,75
2	2,5	0,325	233,77	0,177	281,39	0,093	64,64
3	5,5	0,317	267,35	0,182	290,94	0,138	37,78
4	6	0,316	276,65	0,182	297,32	0,190	21,65
5	9,5	0,316	284,53	0,182	299,59	0,242	13,33

Tab. 3.6. *A-NSIF results along the paths (NW=2, A=-0.5mm, t=0.20mm)*

Path	z	ξ_1	K_I^{App}	ξ_2	K_{II}^{App}	ξ_3	K_{III}^{App}
1	0,5	0,290	261,55	0,189	329,24	0,029	113,81
2	2,5	0,272	341,23	0,198	341,31	0,069	75,18
3	5,5	0,268	378,76	0,201	348,94	0,107	47,25
4	6	0,267	391,12	0,201	355,79	0,150	28,21
5	9,5	0,267	394,33	0,201	358,44	0,191	18,42

Tab. 3.7. *A-NSIF results along the paths (NW=2, A=-1.0mm, t=0.20mm)*

Path	z [mm]	ξ_1	K_I^{App}	ξ_2	K_{II}^{App}	ξ_3	K_{III}^{App}
1	0,5	0,269	376,83	0,234	322,72	0,0001	150,34
2	2,5	0,256	464,63	0,242	330,42	0,026	108,41
3	5,5	0,252	508,97	0,244	340,18	0,040	74,30
4	6	0,252	522,32	0,244	346,47	0,049	53,58
5	9,5	0,252	526,59	0,244	349,02	0,055	42,77

Tab. 3.8. *A-NSIF results along the paths (NW=2, A=-1.5mm, t=0.20mm)*

Path	z	ξ_1	K_I^{App}	ξ_2	K_{II}^{App}	ξ_3	K_{III}^{App}
1	0,5	0,287	458,47	0,285	258,62	0,030	175,18
2	2,5	0,275	551,60	0,293	264,53	0,049	133,02
3	5,5	0,271	599,29	0,295	271,81	0,056	102,43
4	6	0,271	614,14	0,296	275,59	0,059	84,00
5	9,5	0,270	621,65	0,296	277,60	0,061	74,33

Tab. 3.9. *A-NSIF results along the paths (NW=2, A=-2.0mm, t=0.20mm)*

Path	z	ξ_1	K_I^{App}	ξ_2	K_{II}^{App}	ξ_3	K_{III}^{App}
1	0,5	0,323	482,04	0,335	163,82	0,101	181,67
2	2,5	0,310	579,44	0,348	163,74	0,120	145,28
3	5,5	0,306	628,04	0,353	165,79	0,131	121,30
4	6	0,306	643,40	0,354	167,96	0,139	106,56
5	9,5	0,305	651,29	0,354	169,17	0,144	98,90

Tab. 3.10. *A-NSIF results along the paths (NW=2, A=-2.5mm, t=0.20mm)*

Path	z	ξ_1	K_I^{App}	ξ_2	K_{II}^{App}	ξ_3	K_{III}^{App}
1	0,5	0,362	458,36	0,382	68,31	0,182	171,03
2	2,5	0,349	553,79	0,403	64,91	0,202	144,29
3	5,5	0,345	600,81	0,414	63,27	0,215	128,23
4	6	0,344	618,11	0,417	63,33	0,224	118,13
5	9,5	0,344	623,26	0,417	63,75	0,228	113,39

Tab. 3.11. *A-NSIF results along the paths (NW=2, A=-3.0mm, t=0.20mm)*

The tables from Tab. 3.6 to Tab. 3.11 report the a-NSIFs and the singularity degrees of each path for every geometry. Once again, the singularity degrees appear to be constant along the width, even if sometimes the value of the first paths are a bit different from the others; scanning the values of this result, a pattern can be noticed: all the ξ_i values increase when the height of the wave increases with just one exception for the first model, A=-0.5 mm. This fact is no surprise to the ones that already know the notch theory, since a great modification to the surface geometry, like the one that is present in our model, should make the stress distribution more complex.

The trend of the three generalized apparent notch stress intensity factors is different from the one of the singularity degrees: some of them tend to increase when the A parameter increases, some other have an opposite behavior or a mixed one.

To have a better view of these distributions, it is important to plot them into the graphs reported below, which show the variations of K_i^{App} in function of A and of the different paths.

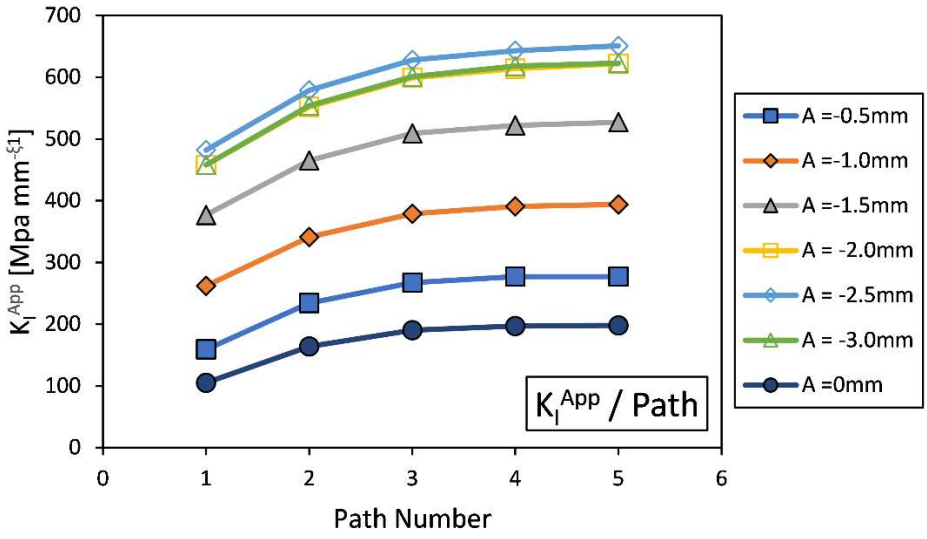

Fig. 3.12. *Graph of K_I^{App} in function of the paths for different heights of wave (NW=2)*

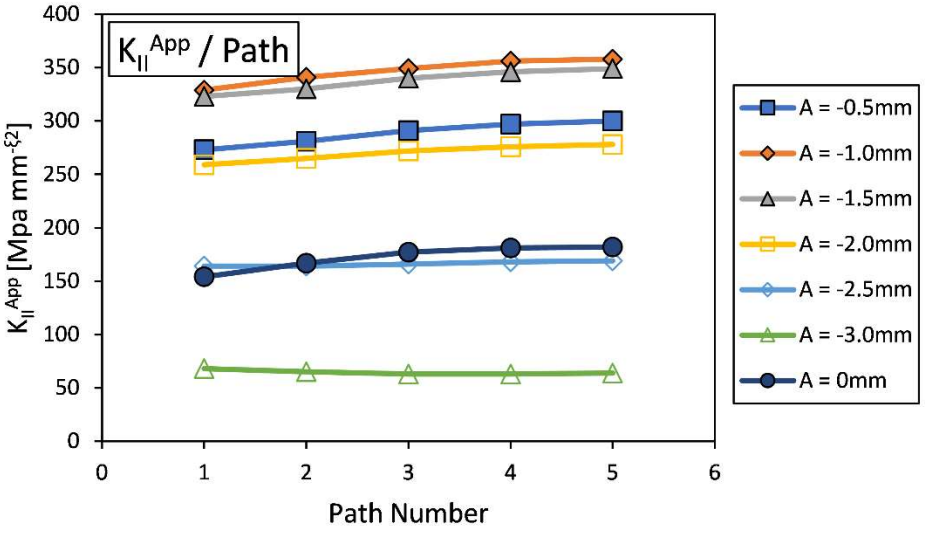

Fig. 3.13. *Graph of K_{II}^{App} in function of the paths for different heights of wave (NW=2)*

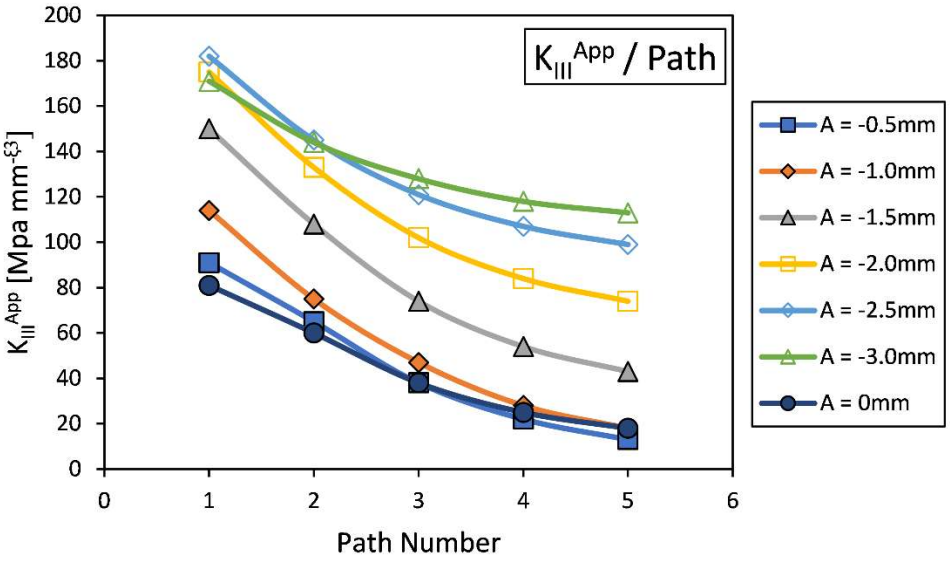

Fig. 3.14. *Graph of K_{III}^{App} in function of the paths for different heights of wave (NW=2)*

Figures from Fig. 3.12 to Fig. 3.14 shows the results of this second analysis, highlighting the differences in terms of apparent generalized notch stress intensity factors between different height of the waves and different path along the width. The first graph shows the trends of K_I^{App}, it's interesting to notice that every geometry shares the same distribution of a-NSIF with the others, making the comparison much clearer: on the bottom of the graph there are the flat geometry and the lower height, A=-0.5 mm, showing that the K_I^{App} increases when the height of the wave grows up. This is true for every value of A except for the highest, A=-3.0 mm, which reports the same a-$NSIF_I$ of A=-2.0 mm; the reason could probably be that the peak is situated between this two heights, and that after this peak the trend is overturned. However, the difference between this value is not so great, thus it is hard to confirm this hypothesis without any further investigation.

Fig. 3.13 also reports that all the geometries follow a similar path: the K_{II}^{App} is almost constant along the width unlike the case of A=0 mm, the flat joint, where the a-$NSIF_{II}$ value increases slightly by moving from the lateral surface to the center of the model. Furthermore, the apparent generalized notch stress intensity factor that represents the in-plane tangential stress diminishes much when the height of the wave increases, down to a minimum around 60-70 MPa for A=-3.0 mm; anyway, the maximum value is not the one corresponding to the minimum of the height because for the lowest sinusoid geometries there is a growing trend and not a waning one. The maximum value is reached with A=-1.0 mm and A=-1.5mm, while the flat model stays once again in the middle of the graph.

Fig. 3.14 lastly shows the trend of K_{III}^{App}, which appears to be similar to the one of K_I^{App}: the maximum value is the one corresponding to A=-3.0 mm and the minimum one corresponds to the minimum height, A=-0.5 mm. The flat joint is situated in the lower part of the image, closer to the geometries with the lower height, and this is another characteristic which is similar to the graph in Fig. 3.12. On the contrary, the trend of each single geometry is the opposite of the one of K_I^{App}, where the value was increasing when moving along the width from the first to the last path; in the case of a-$NSIF_{III}$, this number always decreases from the lateral surface to the middle of the model, losing even the 80% of the initial value for A = 0.5 mm.

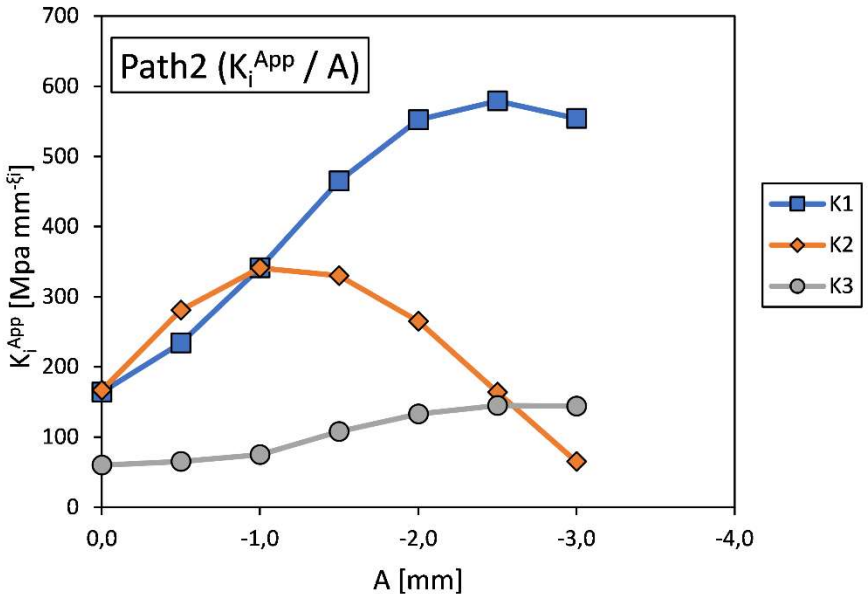

Fig. 3.15. *Graph of K_i^{App} in function of the height of the waves for path 2 (NW=2)*

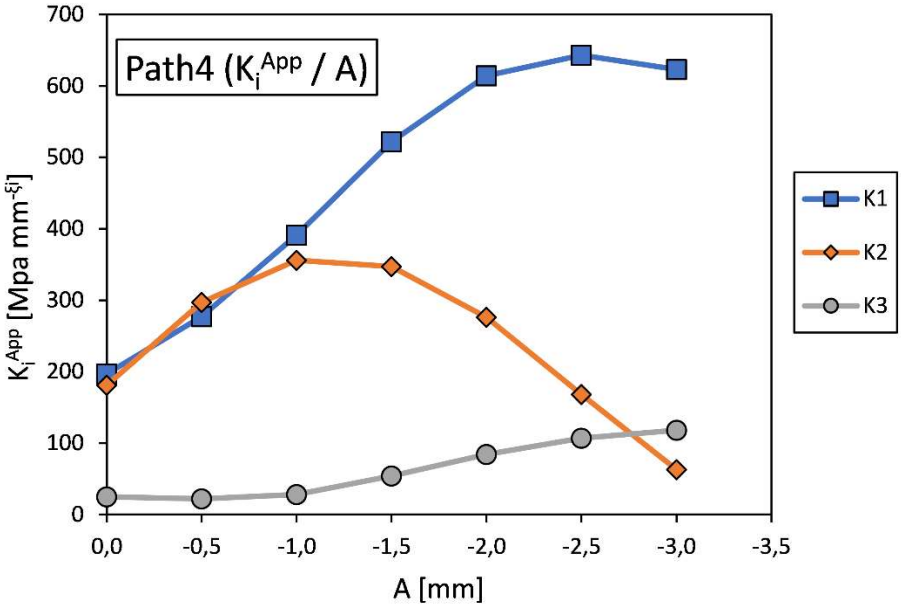

Fig. 3.16. *Graph of K_i^{App} in function of the height of the waves for path 4 (NW=2)*

The last two graphs of this section, Fig. 3.15 and Fig. 3.16, well represent the variation of the three a-NSIF in function of the chosen parameter, the height of the wave. The assessments that can be made are the same that has been explained before, but in this case the trend is even clearer for every single curve. It has to be notice that only two graphs have been reported, path 2 and path 4, because the other three were very similar to them and they wouldn't add any further information. K_I^{APP} and K_{II}^{APP} have a parabolic trend, while K_{III}^{APP} always tends to increase with the growing of A.

3.3 Third parameter: layer thickness

The third parameter used during these simulations is the layer thickness, an analysis similar to the one made by Afshar et al. in [47]. In the flat joint used for comparison the chosen thickness is 0.20 mm, while in the other geometries this value ranges between 0.20 mm and 0.60 mm. The graph in Fig. 3.17 shows the K_I^{APP} factor in function of the five paths for each geometry; the trend is always the same, this a-$NSIF_I$ grows significantly when moving from the first path to the last one, even for the flat geometry. Furthermore, the first apparent generalized notch stress intensity factor increases when the thickness is reduced, up to a maximum for t = 0.20 mm.

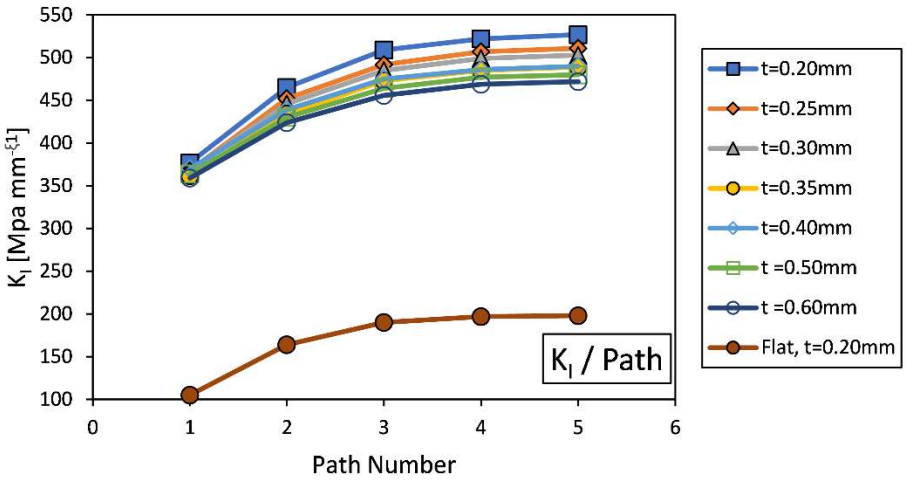

Fig. 3.17. *Graph of K_I^{App} in function of the paths for different layer thickness (NW=2)*

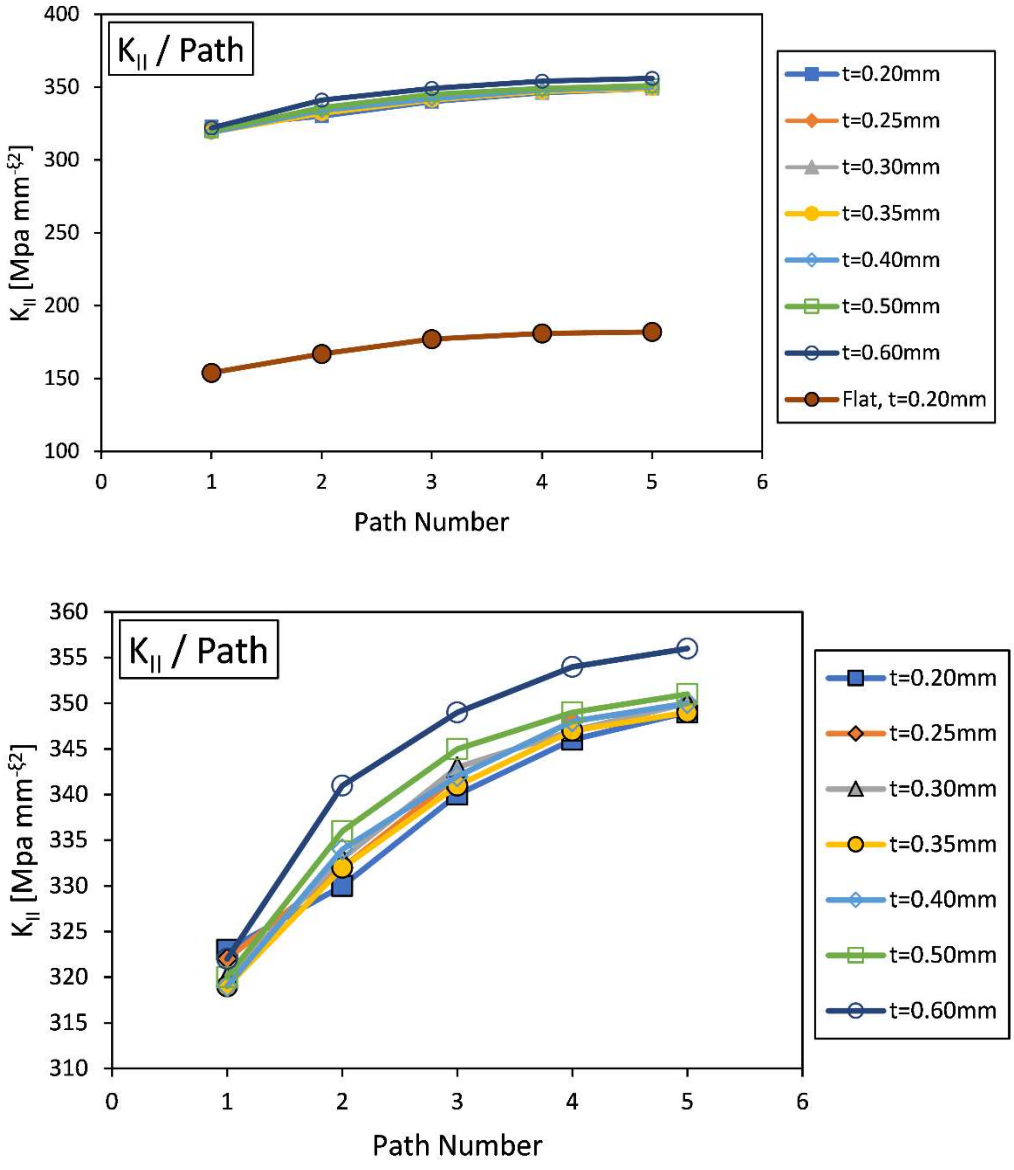

Fig. 3.18. a) *Graph of K_{II}^{App} in function of the paths for different layer thickness (NW=2),*

Fig. 3.18 b) *Same graph without the flat joint*

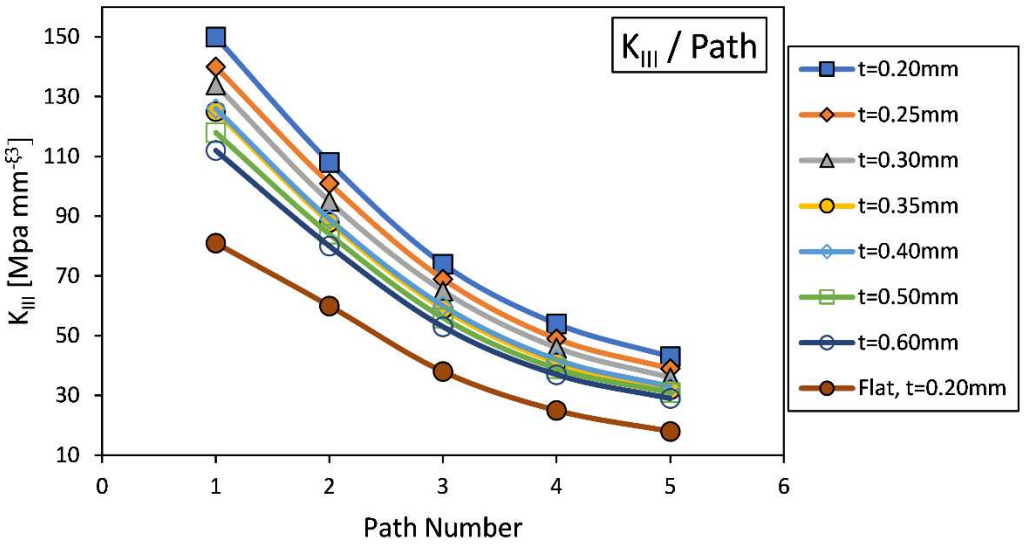

Fig. 3.19. *Graph of K_{III}^{App} in function of the paths for different layer thickness (NW=2)*

Fig. 3.18 (b) underlines the behavior of K_{II}^{App} for the same geometries: the trend of each single geometry is very similar to the one of K_I^{App}, the value grows when moving into the joint from the lateral surface. On the contrary, increasing the adhesive layer's thickness leads to an increase of the factor, unlike what was happening with the first one. In Fig. 3.18 (a) the flat joint has been reported, showing a great increase rise of a-NSIF$_{II}$ when passing from the flat to the wavy geometry.

Lastly, the graph in Fig. 3.19 shows how the last a-NSIF ranges in function of the parameters mentioned above: when moving along the width, the factor tends to decrease, in some cases down to less than 10 percent. A decrease of the layer thickness leads instead to an increase of the third generalized apparent notch stress intensity factor, the one regarding the out-of-plane tangential stress, with a maximum for the t=0.20 mm geometry. The smallest values are the ones collected in the model with the greatest layer thickness and, below all, in the flat joint.

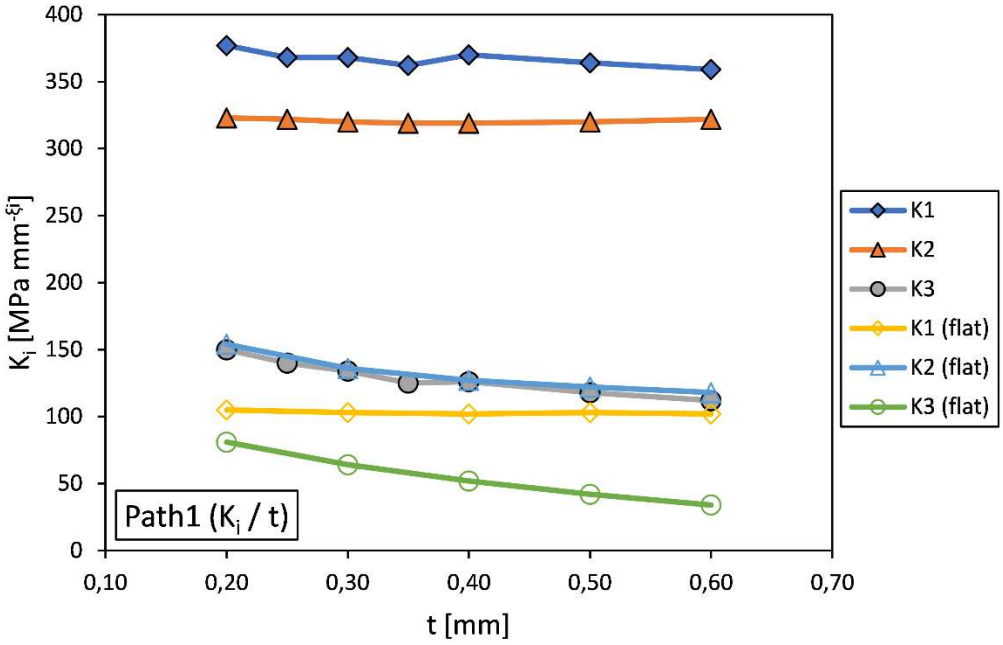

Fig. 3.20. *Graph of K_i^{App} in function of the layer thickness for path 1 (NW=2)*

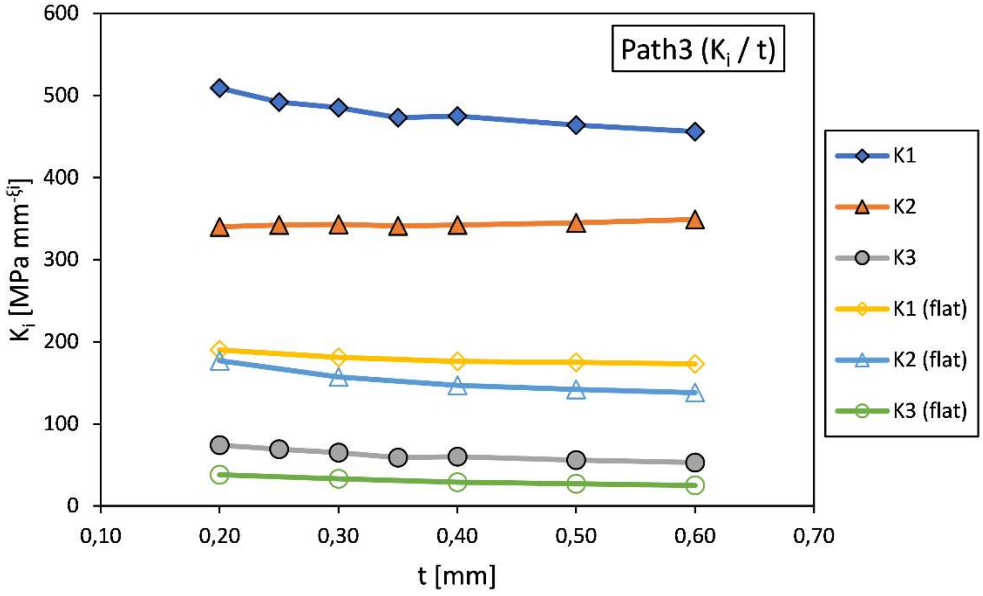

Fig. 3.21. *Graph of K_i^{App} in function of the layer thickness for path 3 (NW=2)*

The last two graphs in Fig. 3.20 and 3.21 are representative of the other point of view, which is the a-NSIF in function of the layer thickness, in both wavy and flat geometries. The other graphs, for path 2, 4 and 5, haven't been reported because they show the same trends of these two. K_I and K_I(flat) show a slight decrease with the increase of the layer thickness, while the other factors seem almost constant but this is due to the scale of each graph, which contains many different values and does not underline the variations of the smallest; for these kind of comparisons it should be better to consider the previous graphs, from Fig. 3.17 to Fig. 3.19, because they show the three apparent generalized notch stress intensity factors separately, making the differences connected to the thickness more evident. In every graph it is evident how the wavy geometry brings to a strong increase of each a-NSIF.

3.4 Fourth parameter: adherent material

The last simulations illustrated in this thesis are the ones that consider the elastic modulus of the adherends as parameter, changing it from 40 GPa to 200 GPa, from the value of a carbon fiber reinforced plastic (50/50 fiber/matrix, biaxial fabric) to the one of a typical steel. In every wavy joint considered in this section the layer thickness is t = 0.2 mm, the number of waves is 4 and the height of the waves is A = -0.5 mm.

Fig. 3.22 shows the K_I^{App} in function of the paths as the Young's modulus varies, underlining how this factor tends to decrease when the parameter increases. The other curve indicated in the following three graphs regards a flat geometry with the same characteristics of the others in terms of layer thickness, adhesive material and joint dimensions, while the elastic modulus of the adherend is set to E = 70 GPa. The values of the flat geometry are much lower than the others but they keep the same tendency. The trend of every single curve is the same that has been encountered before for K_I^{App}, when moving through the thickness the first a-NSIF increases its value in a logarithmic way.

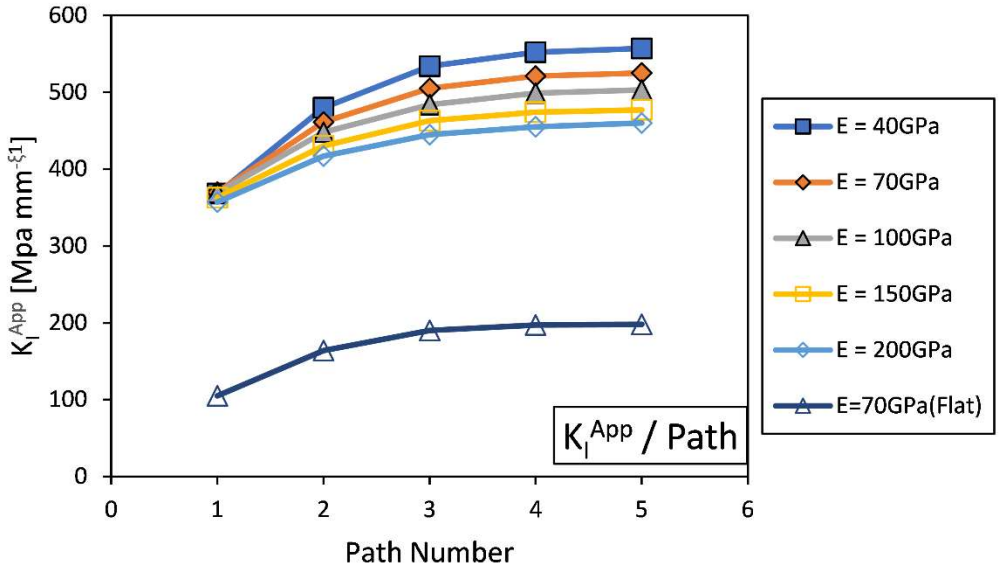

Fig. 3.22. *Graph of K_I^{App} in function of the paths for different Young modules (NW=4)*

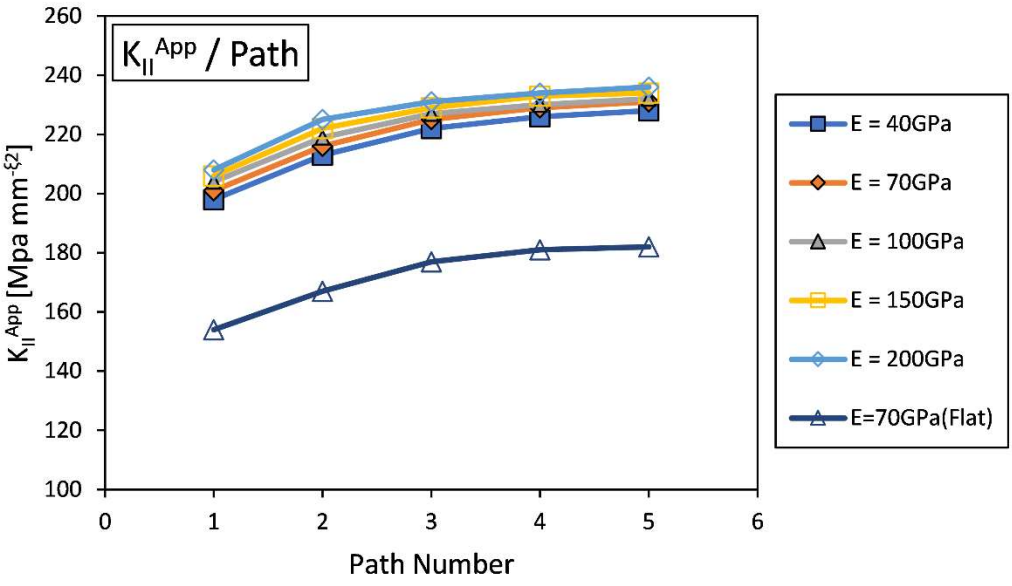

Fig. 3.23. *Graph of K_{II}^{App} in function of the paths for different Young modules (NW=4), with the flat joint*

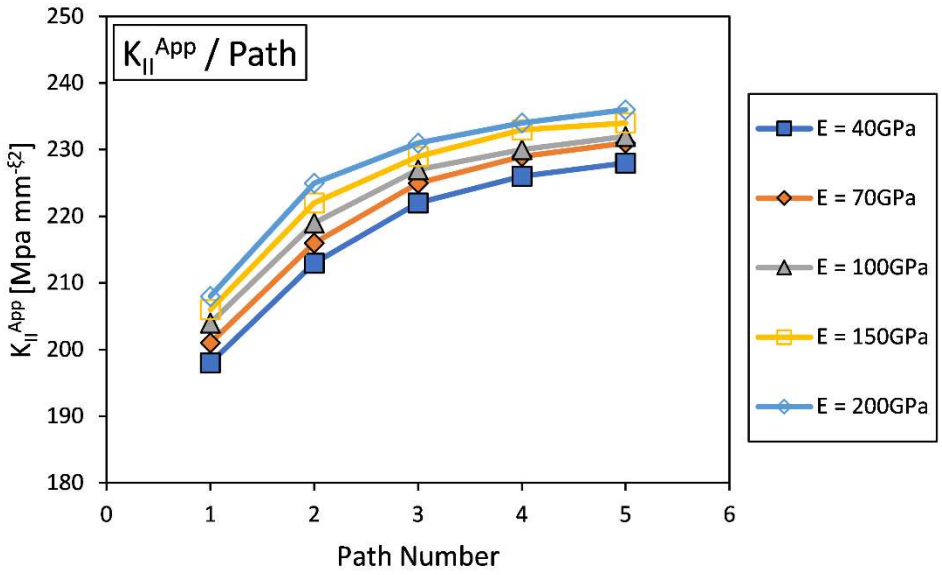

Fig. 3.24. *Graph of K_{II}^{App} in function of the paths for different Young modules (NW=4), without the flat joint*

Fig. 3.23 and 3.24 illustrate the same situation, which is the K_{II}^{App} in function of the Young's modulus of the adherend, but in the second graph the curve related to the flat geometry has been removed to make the other curves clearer. One again the tendency of every single curve is to increase from path 1 to path 5, but this time the influence of the elastic modulus is reversed: in fact, its increasing leads to an increase of the a-NSIF calculated from the tangential in-plane stress. The comparison with a flat geometry shows how the factor is strongly increased when adopting the wavy geometry.

The graph in Fig. 3.25 underlines how the K_{III}^{App} has a similar behavior to K_{I}^{App} when changing the Young's modulus: increase one of them brings to a consequent decrease of the other one. On the other hand, the trend of each curve is the opposite, as previously encountered in all the K_{III}^{App} cases.

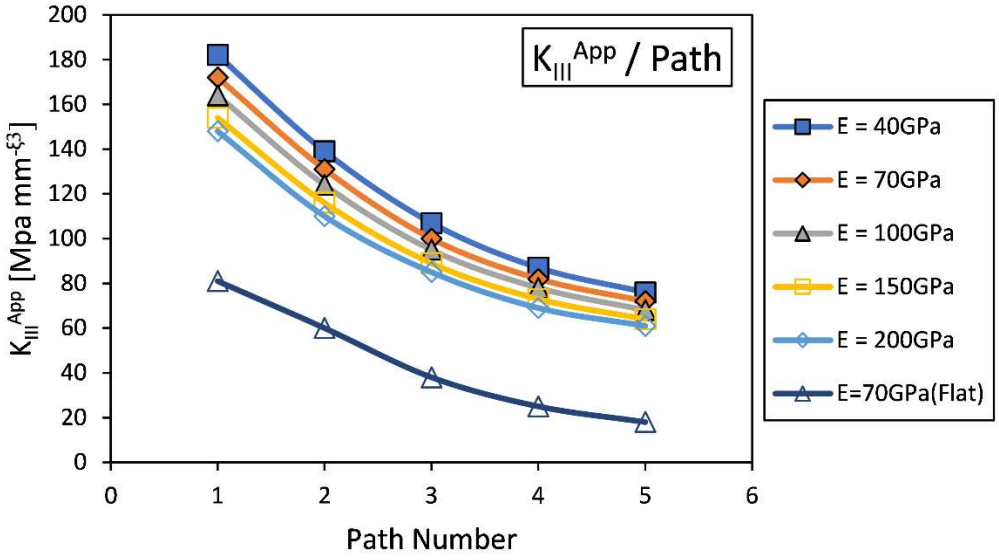

Fig. 3.25. *Graph of K_{III}^{App} in function of the paths for different Young modules (NW=4)*

The last two graphs of this chapter, Fig. 3.26 and Fig. 3.27, report the behavior illustrated above, which are very similar for each of the five paths; this time the curves of a whole flat joint analysis in function of E have been added, showing the differences between them and the ones related to the sinusoidal geometry. As noticed in the previous cases, the wavy joint shows much higher a-NSIFs than the flat joint and another interesting observation can be made on the ratio between K_I^{App} and K_{II}^{App}: in the flat geometry these values are very close to each other, while in the sinusoidal joint there is a huge gap between them.

Lastly, the trend of K_{II}^{App} changes significantly from one geometry to the other, passing from being growing to being decreasing as E increases.

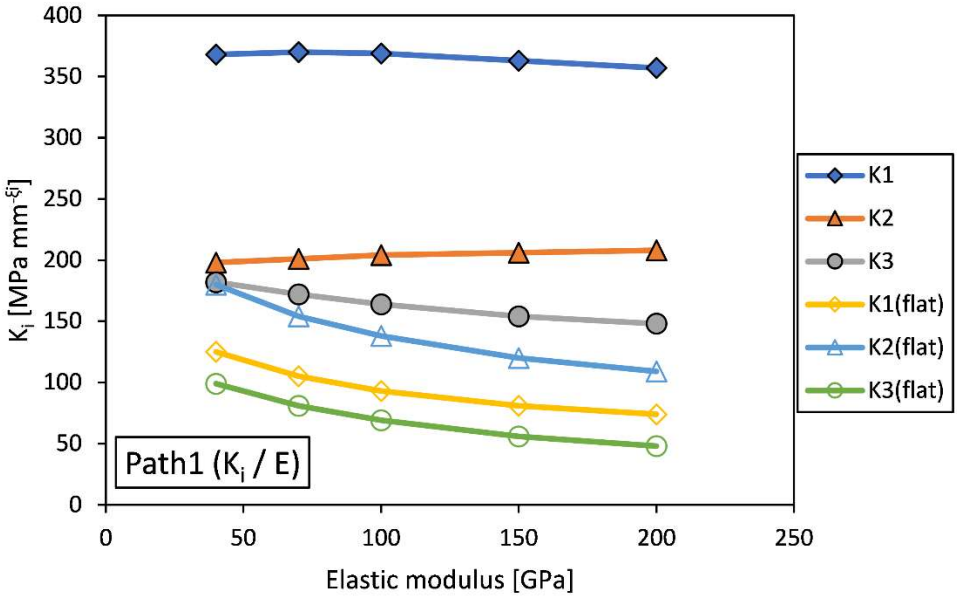

Fig. 3.26. *Graph of K_i^{App} in function of the elastic modulus for path 1 (NW=4)*

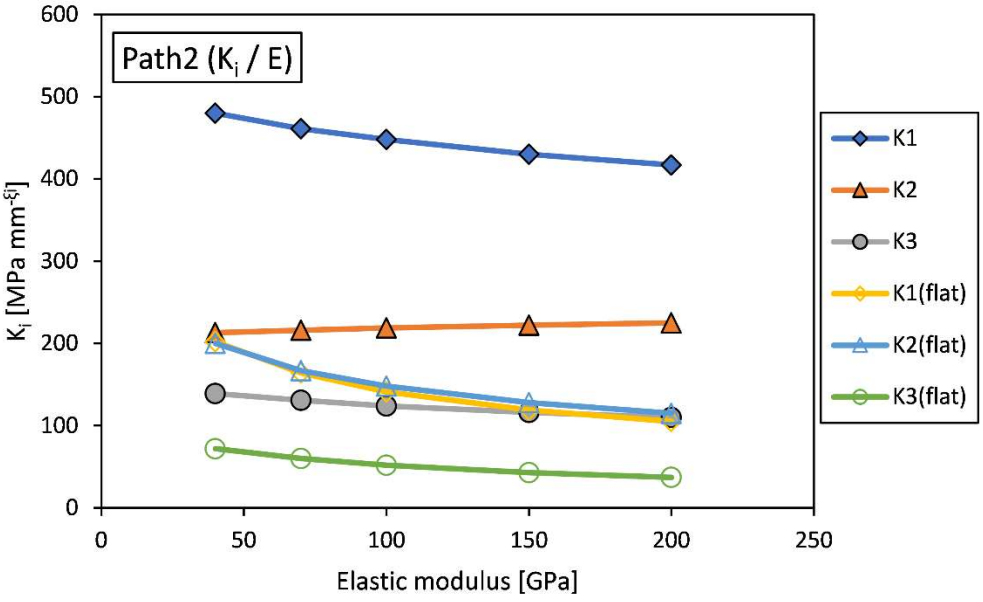

Fig. 3.27. *Graph of K_i^{App} in function of the elastic modulus for path 2 (NW=4)*

Chapter 4

Conclusion and suggestions

This last chapter recapitulates all the considerations made during the whole work and summarizes how the study can be used or where it could be deepened and improved, especially with some experimental data obtained directly in the laboratories.

4.1 Conclusions

From all the analyses conducted up to here, some important deductions can be obtained: the apparent generalized notch stress intensity factors K_i^{App}, calculated from both the in-plane and out-of-plane stress distributions, turned out to be constant in a range of distance from the corner of the joint that goes from 0.5 to 5 mm.

The numerical simulations allowed to get the trends for each one of the four parameters considered:

- Increase the number of waves leads to an increase of K_{III}^{App}, by up to 200% from NW=2 to NW=6 for path 5, and to a decrease of K_I^{App} and K_{II}^{App}, respectively by about 50% and 85%. For K_{II}^{App} the minimum value has been reached for NW=4.
- Increase the height of the sinusoid brings to an increase of K_I^{App} and K_{III}^{App} respectively by up to 200% and 600% (for path 5); K_{II}^{App} instead undergoes a reduction that reaches 85%.
- Increase the thickness of the adhesive layer leads to a very slight increase of K_{II}^{App}, only a few percentage points, while it decreases K_I^{App} of about 20% and K_{III}^{App} of about 50 MPa $mm^{-\xi 3}$; these results are in according to the ones of
- Increase the elastic modulus of the adherent brings to another small increase of K_{II}^{App}, up to 10 MPa $mm^{-\xi 2}$ on a total of about 200 MPa $mm^{-\xi 2}$, and to a decrease of K_I^{App} and of K_{III}^{App}. These last two factor varied by up to 20% and 25% when changing the Young's modulus from 40 GPa to 200 GPa.

- In most of the cases, the aNSIF values for the flat geometry are much lower than the ones regarding the wavy joint, confirming what is in the literature on this subject [58]; the only two exceptions are the K_{II}^{App} for the analyses on length and height of the waves, where the flat values are situated between the ones of the sinusoid cases.

4.2 Proposals

As mentioned at the real beginning of this project, this work is not meant to be fully exhaustive; in fact, there is more than one aspect that could be studied in deep, introducing for example different Young modules or Poisson's ratios for the adherend, even if some previous papers already did it, like that by Afshar et al. [47].

Another important factor that has not been introduced in this thesis is the experimental one: it would be of great interest to have some experimental data in support of the finite elements simulation done during this research. These data could confirm the simulations reported above or they could open a new discussion and introduce some new factors and issues.

The analysis of different ways to stress the joint could also be interesting, especially some fatigue analyses which are fundamental for the study of a bonded joint, usually subject of an high number of cycles.

Nomenclature

A	=	Height of the waves
B	=	Length of a single wave
Ki^{App}	=	Apparent generalized notch stress intensity factor
L	=	Length of the joint
r	=	Distance from the left corner of the joint
t	=	Thickness of the adhesive layer

Greek letters

ξ	=	Singularity degree
σ	=	Peel stresses
τ	=	Shear stresses
ϑ	=	Angle of adhesive layer

Acronyms

FE	=	Finite Elements
FPZ	=	Fracture Process Zone
FRP	=	Fiber-Reinforced Plastic
NSIF	=	Notch Stress Intensity Factor
NW	=	Number of Waves
RAM	=	Random Access Memory
SED	=	Strain Energy Density
SEM	=	Scanning Electron Microscope
SLJ	=	Single Lap Joint

References

[1] Berto F., Lazzarin P., A review of the volume-based strain energy density approach applied to V-notches and welded structures, Theoretical and Applied Fracture Mechanics 52, 183-194 (2009)

[2] Davis M., Bond D., Principles and practices of adhesive bonded structural joints and repairs, International Journal of Adhesion and Adhesives 19, 91-105 (1999)

[3] Sheppard A., Kelly D., Tong L., A damage zone model for the failure analysis of adhesively bonded joints, International Journal of Adhesion and Adhesives 18, 385-400 (1998)

[4] Benyus J.M., Biomimicry: innovation inspired by nature, New York: William Morrow Paperbacks (2002)

[5] Lenau T., Barfoed M., Material innovation ispired by nature, Dansk Metallurgisk Selskab: Vintermodet, Byggecentrum Middelfart, 103-112 (2007)

[6] Barthelat F., Espinosa H., An experimental investigation of deformation and fracture of nacre-mother of pearl, Experimental Mechanics 47, 311-324 (2007)

[7] Xiaocong H., A review of finite element analysis of adhesively bonded joints, International Journal of Adhesion and Adhesives 31, 248-264 (2011)

[8] Belingardi G., Goglio L., Tarditi A, Investigating the effect of spew and chamfer size on the stresses in metal/plastic adhesive joints, International Journal of Adhesion and Adhesives, 22, 273-282 (2002)

[9] Cooper P.A., Sawyer J.W., A critical examination of stresses in an elastic single lap joint, NASA Technical paper 1507 (1979)

[10] Erdogan F., Ratwani M., Stress distribution in bonded joints, Journal of Composite Materials, 5, 378-393, (1971)

[11] Renton W.J., Vinson J.R., The Efficient Design of Adhesive Bonded Joints, The Journal of Adhesion, 7, 175-193 (1974)

[12] Akpinar S., Aydin M.D., Ozel A., A study on 3-D stress distributions in the bi-adhesively bonded T-joints, Applied Mathematical Modelling,37, 10220-10230 (2013)

[13] Khoramishad H., Razavi S.M.J., Metallic fiber-reinforced adhesively bonded joints, International Journal of Adhesion and Adhesives, 55, 114-122 (2014)

[14] Gultekin K., Akpinar S., Gurses A., Eroglu Z., Cam S., Akbulut H., Keskin Z., Ozel A., The effects of graphene nanostructure reinforcement on the adhesive method and the graphene reinforcement ratio on the failure load in adhesively bonded joints, The Journal of Adhesion, 98, 362-369 (2016)

[15] Ayatollahi M.R., Nemati Giv A., Razavi S.M.J., Khoramishad H., Mechanical properties of adhesively single lap bonded joints reinforced with multi-walled carbon nanotubes and silica nanoparticles, The Journal of Adhesion, 13 May 2016 (Peer Reviewed Journal)

[16] Esmaeili E., Razavi S.M.J., Bayat M., Berto F., Flexural behavior of metallic fiber-reinforced adhesively bonded single lap joints, The Journal of Adhesion, (in press - 2017)

[17] Aydin M.D., Akpinar S., The strength of the adhesively bonded T-joints with embedded supports, International Journal of Adhesion and Adhesives, 50, 142-150 (2014)

[18] Doru M.O., Ozel A., Akpinar S., Aydin M.D., Effect of the Spew Fillet on Adhesively Bonded Single-Lap Joint Subjected to Tensile Loading: Experimental and 3-D Non-Linear Stress Analysis, The Journal of Adhesion, 90, 195-209 (2014)

[19] Akpinar S., The strength of the adhesively bonded step-lap joints for different step numbers, Composites Part B: Engineering, 67, 170-178 (2014)

[20] Da Silva L.F.M., Handbook of Adhesion Technology, 689-723 (2011)

[21] Adhesive and Sealants, Engineered Materials Handbook, Vol.3, (ASM International, 1990)

[22] Adhesive Bonding Handbook for Advanced Structural Materials, (European Space Research and Technology Centre, European Space Agency, Noordwjik, Netherlands, 1990)

[23] Hildebrand M., Non-linear analysis and optimization of adhesively bonded single lap joints between fibre-reinforced plastics and metals, International Journal of Adhesion and Adhesives, 14, 261-267 (1994)

[24] Razavi S.M.J., Esmaeili E., Samari M., Razavi S.M.R., Stress analysis on a non-flat zigzag interface bonded joint, The Journal of Adhesion, (in press - 2017)

[25] Boss J.N., Ganesh V.K., Lim C.T., Modulus grading versus geometrical grading of composite adherends in single-lap bonded joints, Composites Structures, 62, 113-121 (2003)

[26] McLaren A.S., MacInnes I., The influence on the stress distribution in an adhesive lap joint of bending the adhering sheets, British Journal of Applied Physics, 9, 72-77 (1958)

[27] Fessel G., Broughton J.G., Fellows N.A., Durodola J.F., Hutchinson A.R., A Numerical and Experimental Study on Reverse-Bent Joints for Composite Substrates. 48th AIAA/ASME/ASCE/AHS/ASC Structures, Structural Dynamics, and Materials Conference, Honolulu, Hawaii (2007)

[28] Fessel G., Broughton J.G., Fellows N.A., Durodola J.F., Hutchinson A.R., Fatigue performance of metallic reverse-bent joints, Fatigue & Fracture of Engineering Materials & Structures, 32, 704-712 (2009)

[29] Campilho R.D.S.G., Pinto A.M.G., Banea M.D., Silva R.F., da Silva L.F.M., Strength Improvement of Adhesively-Bonded Joints Using a Revers-Bent Geometry, Journal of Adhesion Science and Technology, 25, 2351-2368 (2001)

[30] You M., Li Z., Zheng X., Yu S., Li G., Sun D., A numerical and experimental study of preformed angle in the lap zone on adhesively bonded steel single lap joint, International Journal of Adhesion and Adhesives, 29, 280-285 (2009)

[31] Zeng Q., Sun C.T., A New Bonded Composite Wavy Lap Joint, 41st AIAA/ASME/ASCE/AHS/ASC Structures, Structural Dynamics, and Material Conference, Atlanta, Georgia, US (2000)

[32] Zeng Q., Sun C.T., Novel Design of a Bonded Lap Joint, AIAA J., 39, 1991-1996 (2001)

[33] Zeng Q., Sun C.T., Fatigue performance of a Bonded Wavy Composite Lap Joint, Fatigue & Fracture of Engineering Materials & Structures 27, 413-422 (2004)

[34] Zeng Q., Sun C.T., Fatigue performance of a Bonded Wavy Composite Lap Joint, 42nd AIAA/ASME/ASCE/AHS/ASC Structures, Structural Dynamics, and Material Conference, Seattle, Washington, US (2001)

[35] Avila A.F., Bueno P.O., Stress analysis on a wavy-lap joint for composites, International Journal of Adhesion and Adhesives 24, 407-414 (2003)

[36] Shiva Shankar G.S., Vijayarangan S., Krishna N.S., Failure analysis of Lap and Wavy-Lap Composite Bonded Joints, Proceeding of the International Symposium of Research Students on Material Science and Engineering (2004), pp. 1-8

[37] Fessel G., Broughton J.G., Fellow N.A., Durodola J.F., Hutchinson A.R., Evaluation of different lap-shear joint geometries for automotive applications, International Journal of Adhesion and Adhesives 27, 574-583 (2007)

[38] De Moura M.F.S.F., Gonçalves J.P.M., Chousal J.A.G., Campilho R.D.S.G., Cohesive and continuum mixed-mode damage models applied to the simulation of the mechanical behavior of bonded joints, International Journal of Adhesion and Adhesives 28, 419-426 (2008)
[39] Temiz S., Akpinar S., Aydin M.D., Sancaktar E., Increasing single-lap joint strength by a adherend curvature induced residual stresses, Journal of Adhesion Science and Technology 27, 244-251 (2013)
[40] Akpinar S., Effects of Different Curvature Patches on the Strength of Double-Strap Adhesive Joints, Journal of Adhesion 89, 937-947 (2013)
[41] Niem P.I.F., Lau T.L., Kwan K.M., The effect of surface characteristics of polymeric materials on the strength of bonded joints, Journal of Adhesion Science and Technology 10, 361-372 (1996)
[42] Ashrafi M., Ajdari A. Rahbar N., Papadopoulos J., Nayeb-Hashemi H., Vaziri A., Adhesively bonded single lap joints with non-flat interfaces, International Journal of Adhesion and Adhesives 32, 46-52 (2012)
[43] Haghpanah B., Chiu S., Vaziri A., Adhesively bonded lap joints with extreme interface geometry, International Journal of Adherents and Adhesives 48, 130-138 (2014)
[44] Berto F., Marangon C., Three-dimensional effects in finite thickness plates weakened by rounded notches and holes under in-plane shear, Fatigue & Fracture of Engineering Materials & Structures 36, 1139-1152 (2013)
[45] Richardson G., Crocombe A.D., Smith P.A., A comparison of two- and three-dimensional finite element analysis of adhesive joints, International Journal of Adhesion and Adhesives 13, 193-200 (1993)
[46] Ewalds H.L., Wanhill R.J.H., Fracture Mechanics, Edward Arnold and Delftse Uitgevers Maatschappij, 1984
[47] Afshar R., Berto F., Lazzarin P., Three-dimensional finite element analysis of single-lap joints: effect of adhesive thickness and Poisson's ratio, Kay Engineering Materials 577-578, 393-396 (2014)
[48] da Silva L.F.M., das Neves P.J.C., Adams R.D., Spelt J.K., Analytical models of adhesively bonded joints – Part I: Literature survey, International Journal of Adhesion and Adhesives 29, 319-330 (2009)

[49] da Silva L.F.M., das Neves P.J.C., Adams R.D., Spelt J.K., Analytical models of adhesively bonded joints – Part II: Comparative study, International Journal of Adhesion and Adhesives 29, 331-341 (2009)
[50] Bogdanovich A.E., Kizhakkethara I., Three-dimensional finite element analysis of double-lap composite adhesive bonded joint using submodeling approach, Composites Part B: Engineering 30, 537-551 (1999)
[51] Gonçalves J.P.M., de Moura M.F.S.F., de Castro P.M.S.T., A three-dimensional finite element model for stress analysis of adhesive joints, International Journal of Adhesion and Adhesives 22, 357-365 (2002)
[52] Pandey P.C., Narasimhan S., Maruthi Pavan P.V.R., Three dimensional viscoplastic analysis of adhesively bonded lap joints, Proc Eighth National Sem Aerospace Struct (NASAS-8), 135-142 (1998)
[53] Pandey P.C., Narasimhan S., Three dimensional viscoplastic and geometrically nonlinear finite element analysis of adhesively bonded single lap joints, ARDB Report No Aero/RD-134/100/10/96-97/924, Dept Civil Engng, Indian Institute of Science, Bangalore (1999)
[54] Narasimhan S., Three dimensional viscoplastic and geometrically nonlinear finite element analysis of adhesively bonded joints, MSc Thesis, Dept Civil Engng, Indian Institute of Science, Bangalore, 1998
[55] Pandey P.C., Narasimhan S., Three-dimensional nonlinear analysis of adhesively bonded lap joints considering viscoplasticity in adhesives
[56] Gross B., Mendelson A., Plane elastostatic analysis of V-notched plates, International Journal of Fracture Mechanics 8, 267-276 (1972)
[57] Berto F., Campagnolo A., Pook L.P., Three-dimensional effects on cracked discs and plates under nominal Mode III loading, Frattura ed integrità strutturale 34, 190-199 (2015)
[58] Ayatollahi M.R., Samari M., Razavi S.M.J., Da Silva L.F.M., Fatigue performance of adhesively bonded single lap joints with non-flat sinusoid interfaces, Fatigue & Fracture of Engineering Materials & Structures, Published Online (2016)

Websites

www.matweb.com

www.olympus-ims.com

www.matweb.com

www.sciencedirect.com